A simulation study of Li-ion batteries based on a modified P2D model

Author

Name: Zihao Yu

Affiliation: Shenzhen International Graduate School, Tsinghua University

Address: Shenzhen, China

Postcode: 518055

Name: Yao Tian

Affiliation: Shenzhen International Graduate School, Tsinghua University

Address: Shenzhen, China

Postcode: 518055

Corresponding author

Name: Baohua Li

Affiliation: Shenzhen International Graduate School, Tsinghua University

Address: Shenzhen, China

Postcode: 518055

Email: libh@mail.sz.tsinghua.edu.cn

HIGHLIGHTS

· P2D model is modified for application.

· An algorithm for computing the parameters of the modified P2D model is developed.

· An algorithm for computing the outputs of the modified P2D model is developed.

ABSTRACT

Li-ion batteries are used widely in electric vehicles and electronic devices. Pseudo 2-Dimensional model(P2D model) is a classical physics-based Li-ion battery model and it is used widely for its high accuracy. In this paper, P2D model is modified for application. To compute the parameters and outputs of the modified P2D model fast and accurately, algorithms for computing the parameters and outputs of the modified P2D model are developed. To assess the effectiveness of the modified P2D model and the algorithms for computing the parameters and outputs of the modified P2D model, experiments

and simulations are conducted. The experiments are conducted to obtain the data for conducting the simulations and the simulations are conducted based on the modified P2D model and the algorithms for computing the parameters and outputs of the modified P2D model. According to the simulation results, the modified P2D model and the algorithms for computing the parameters and outputs of the modified P2D model are effective. The modified P2D model and the algorithms for computing the parameters and outputs of the modified P2D model can be used to develop Li-ion battery charging methods.

Keywords: Li-ion battery; P2D model; algorithm; simulation; MATLAB

1. Introduction

Li-ion batteries have been commercialized in 1991 and used widely in electric vehicles and electronic devices for their high energy density, high power density and excellent cycle performance [1-6]. In the long run, the uses of Li-ion battery models include controlling the outputs of Li-ion batteries and optimizing the parameters of Li-ion batteries, which means Li-ion battery models can promote the proper utilization and directional improvement of Li-ion batteries. There are three kinds of Li-ion battery models: physics-based Li-ion battery models, data-driven Li-ion battery models and equivalent-circuit Li-ion battery models [7-12]. Physics-based Li-ion battery models can be seen as the organized systems of physical equations and chemical equations, which means the values of the parameters of Li-ion batteries can be assigned to their parameters and it provides the precondition for the uses of physics-based Li-ion battery models in optimizing the parameters of Li-ion batteries.

In the study of physics-based Li-ion battery models, P2D model is a milestone, which is developed in 1993 and used widely for its high accuracy [13-16]. P2D model takes a Li-ion battery load current as its input and Li-ion battery inter-electrode potential of as its output. The Li-ion battery inter-electrode potential equals to the sum of the Li-ion battery open circuit potential, Li-ion battery ohm overpotential, Li-ion battery activation overpotential and Li-ion battery concentration overpotential. The sub-models of P2D model for computing the lithium concentration in Li-ion battery electrode particles and the Li^+ concentration in Li-ion battery electrolytes are 1-dimensional models. Additionally, the process of computing the lithium concentration in Li-ion battery electrode particles is independent of the process of computing the Li^+ concentration in Li-ion battery electrolytes. Therefore, P2D model is not a real 2-dimensional model but a pseudo 2-dimensional model. Modified from or coupled with P2D model, different physics-based Li-ion battery models like SP model and electrochemical-thermal model are derived to meet different requirements [17-22]. Reducing the complexity of full-order physics-based Li-ion battery models or improving the accuracy of reduced-order physics-based Li-ion battery models are two typical ways of modifying physics-based Li-ion battery models. Essentially, both reducing the complexity of full-order physics-based

Li-ion battery models and improving the accuracy of reduced-order physics-based Li-ion battery models are making a compromise between the speed and accuracy of computation. Therefore, reducing the complexity of full-order physics-based Li-ion battery models or improving the accuracy of reduced-order physics-based Li-ion battery models is not a permanent solution. Given a physics-based Li-ion battery model, algorithms for computing its parameters and outputs determine how fast and accurately its parameters and outputs are computed. Therefore, algorithms for computing the parameters and outputs of the physics-based Li-ion battery models are worthy of study.

In this paper, P2D model is modified for application. To compute the parameters and outputs of the modified P2D model fast and accurately, algorithms for computing the parameters and outputs of the modified P2D model are developed. To assess the effectiveness of the modified P2D model and the algorithms for computing the parameters and outputs of the modified P2D model, experiments and simulations are conducted. The experiments are conducted to obtain the data for conducting the simulations and the simulations are conducted based on the modified P2D model and the algorithms for computing the parameters and outputs of the modified P2D model. According to the simulation results, the modified P2D model and the algorithms for computing the parameters and outputs of the modified P2D model are effective. The modified P2D model and the algorithms for computing the parameters and outputs of the modified P2D model can be used to develop Li-ion battery charging methods. The nomenclature of this paper is given in Appendix A.

2. Modified P2D model

In this chapter, P2D model is modified for application. Fig. 1 shows the coordinate system and block diagram of the modified P2D model.

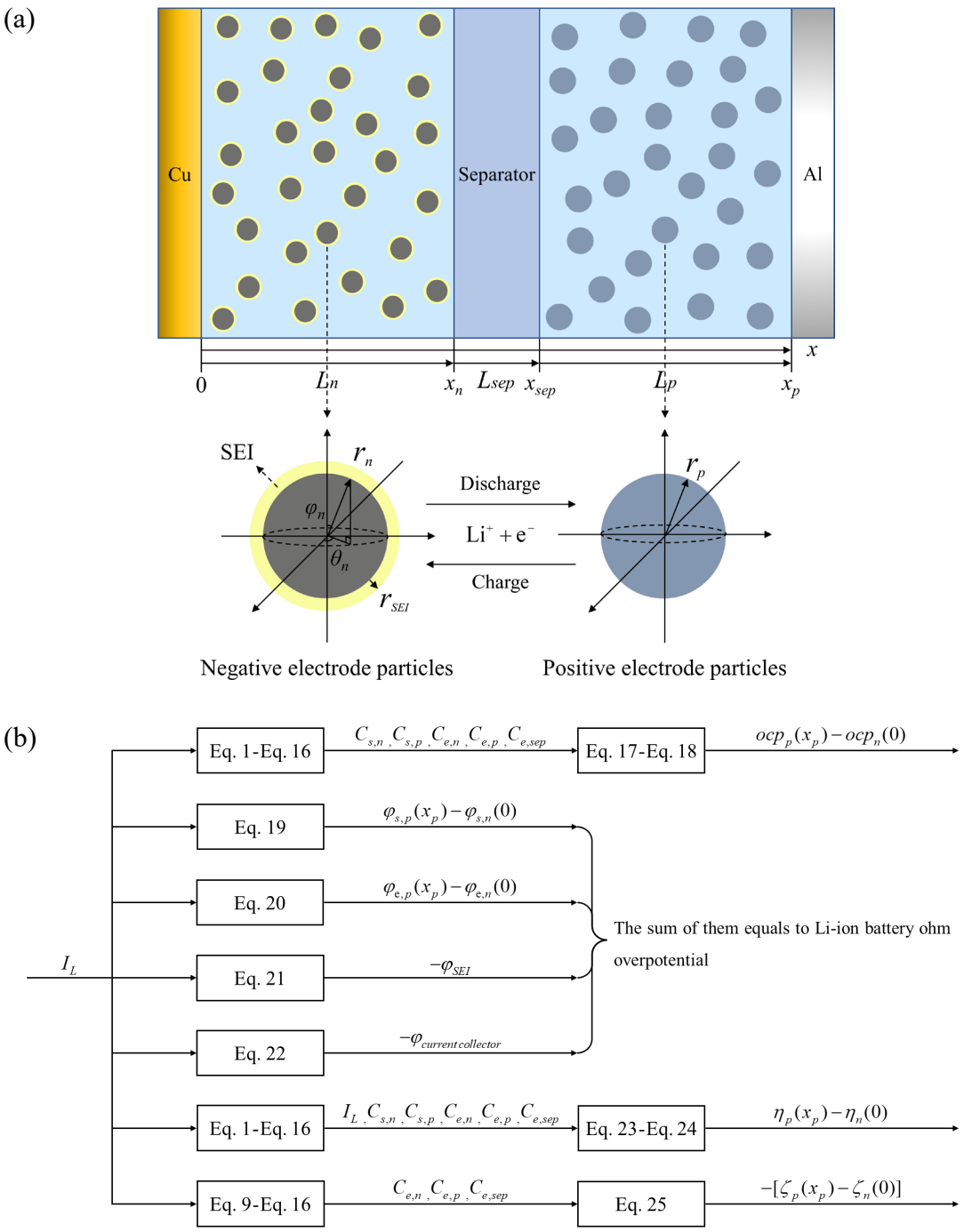

Fig. 1. (a) The coordinate system of the modified P2D model. (b) The block diagram of the modified P2D model.

According to Fig. 1b, the modified P2D model can be seen as the organized system of Eq. 1-Eq. 25 and it takes a Li-ion battery load current as its input and Li-ion battery

inter-electrode potential of as its output. Let the reference directions of Li-ion battery load currents, Li-ion battery electrode currents and Li-ion battery electrolyte currents be along *x* axis. After then, Eq. 1-Eq. 25 are derived and written as below.

Based on Fick's Second Law, the partial differential equations for computing the lithium concentration in Li-ion battery electrode particles are derived and written as

$$\frac{\partial C_{s,n}}{\partial t} = D_{s,n}\left(\frac{\partial^2 C_{s,n}}{\partial r_n^{\,2}} + \frac{2}{r_n}\frac{\partial C_{s,n}}{\partial r_n}\right) \tag{1}$$

$$\frac{\partial C_{s,p}}{\partial t} = D_{s,p}\left(\frac{\partial^2 C_{s,p}}{\partial r_p^{\,2}} + \frac{2}{r_p}\frac{\partial C_{s,p}}{\partial r_p}\right) \tag{2}$$

The initial conditions are written as

$$C_{s,n}\Big|_{t=0} = C_{s,n,initial} \tag{3}$$

$$C_{s,p}\Big|_{t=0} = C_{s,p,initial} \tag{4}$$

The boundary conditions are written as

$$-D_{s,n}\frac{\partial C_{s,n}}{\partial r_n}\Big|_{r_n=0} = 0 \tag{5}$$

$$-D_{s,p}\frac{\partial C_{s,p}}{\partial r_p}\Big|_{r_p=0} = 0 \tag{6}$$

$$-D_{s,n}\frac{\partial C_{s,n}}{\partial r_n}\Big|_{r_n=R_n} = \frac{I_L}{a_n S_n L_n n_+ F} \tag{7}$$

$$-D_{s,p}\frac{\partial C_{s,p}}{\partial r_p}\Big|_{r_p=R_p} = -\frac{I_L}{a_p S_p L_p n_+ F} \tag{8}$$

Given a Li-ion battery load current, Eq. 1-Eq. 8 are used to compute the lithium concentration in Li-ion battery electrode particles.

Based on Fick's First Law, the partial differential equations for computing the Li^+ concentration in Li-ion battery electrolytes are derived and written as

$$\frac{\partial C_{e,n}}{\partial t} = D_e\frac{\partial^2 C_{e,n}}{\partial x^2} + \frac{(1-t_+)I_L}{\varepsilon_{e,n} S_n L_n n_+ F} \tag{9}$$

$$\frac{\partial C_{e,p}}{\partial t} = D_e \frac{\partial^2 C_{e,p}}{\partial x^2} - \frac{(1-t_+) I_L}{\varepsilon_{e,p} S_p L_p n_+ F} \tag{10}$$

$$\frac{\partial C_{e,sep}}{\partial t} = D_e \frac{\partial^2 C_{e,sep}}{\partial x^2} \tag{11}$$

The initial conditions are written as

$$C_{e,n}\Big|_{t=0} = \overline{C_e} \tag{12}$$

$$C_{e,p}\Big|_{t=0} = \overline{C_e} \tag{13}$$

$$C_{e,sep}\Big|_{t=0} = \overline{C_e} \tag{14}$$

The boundary conditions are written as

$$-D_e \frac{\partial C_{e,n}}{\partial x}\Big|_{x=0} = 0 \tag{15}$$

$$-D_e \frac{\partial C_{e,p}}{\partial x}\Big|_{x=x_p} = 0 \tag{16}$$

Given a Li-ion battery load current, Eq. 9-Eq. 16 are used to compute the Li^+ concentration in Li-ion battery electrolytes.

Based on Nernst Equation, the equations for computing Li-ion battery open circuit potential are derived and written as

$$ocp_n(0) = \frac{(\mu^{\circ}_{Li^+} + \mu^{\circ}_{\theta_{s,n}} - \mu^{\circ}_{Li\text{-}\theta_{s,n}}) + RT[\ln C_{e,n}(0) + \ln(C_{s,n,max} / C^{surf}_{s,n} - 1)]}{n_+ F} \tag{17}$$

$$ocp_p(x_p) = \frac{(\mu^{\circ}_{Li^+} + \mu^{\circ}_{\theta_{s,p}} - \mu^{\circ}_{Li\text{-}\theta_{s,p}}) + RT[\ln C_{e,p}(x_p) + \ln(C_{s,p,max} / C^{surf}_{s,p} - 1)]}{n_+ F} \tag{18}$$

Given the lithium concentration in Li-ion battery electrode particles, Eq. 17-Eq. 18 are used to compute Li-ion battery open circuit potential.

Based on Ohm's Law, the equation for computing Li-ion battery electrode ohm overpotential is derived and written as

$$\varphi_{s,p}(x_p) - \varphi_{s,n}(0) = -k_{s,t} \cdot \left(\frac{I_L L_n}{2\sigma_n \varepsilon_{s,n} S_n} + \frac{I_L L_p}{2\sigma_p \varepsilon_{s,p} S_p}\right) \tag{19}$$

Given a Li-ion battery load current, Eq. 19 is used to compute Li-ion battery electrode ohm overpotential. For Li-ion battery electrodes, it is the extension of their

electronic conduction paths but not the decreases of their electronic conductivities caused by the tortuosity of their electronic conduction paths. Instead of Bruggeman coefficient, $k_{s,t}$ is introduced to modify the equation for computing Li-ion battery electrode ohm overpotential. $k_{s,t}$ is a proportional coefficient and $k_{s,t} > 1$.

Based on Ohm's Law, the equation for computing Li-ion battery electrolyte ohm overpotential is derived and written as

$$\varphi_{e,p}(x_p) - \varphi_{e,n}(0) = -k_{e,t} \cdot \left(\frac{I_L L_n}{2\kappa\varepsilon_{e,n} S_n} + \frac{I_L L_p}{2\kappa\varepsilon_{e,p} S_p} + \frac{I_L L_{sep}}{\kappa\varepsilon_{e,sep} S_{sep}}\right) \tag{20}$$

Given a Li-ion battery load current, Eq. 20 is used to compute Li-ion battery electrolyte ohm overpotential. For Li-ion battery electrolytes, it is the extension of their ionic conduction paths but not the decreases of their ionic conductivities caused by the tortuosity of their ionic conduction paths. Instead of Bruggeman coefficient, $k_{e,t}$ is introduced to modify the equation for computing Li-ion battery electrolyte ohm overpotential. $k_{e,t}$ is a proportional coefficient and $k_{e,t} > 1$.

Based on Ohm's Law, the equation for computing SEI ohm overpotential is derived and written as

$$-\varphi_{SEI} = -\frac{I_L R_n R_{SEI}}{\sigma_{SEI} a_n S_n L_n (R_n + R_{SEI})} \tag{21}$$

Given a Li-ion battery load current, Eq. 21 is used to compute SEI ohm overpotential.

Based on Ohm's Law, the equation for computing Li-ion battery current collector ohm overpotential is derived and written as

$$-\varphi_{current\ collector} = -I_L R_{current\ collector} \tag{22}$$

Given a Li-ion battery load current, Eq. 22 is used to compute Li-ion battery current collector ohm overpotential.

Based on Butler-Volmer Equation, the equations for computing Li-ion battery activation overpotential are derived and written as

$$\frac{I_L}{a_n S_n L_n n_+ F} = \{\exp[\frac{(1-\alpha_n) n_+ F \eta_n(0)}{RT}] - \exp[-\frac{\alpha_n n_+ F \eta_n(0)}{RT}]\} k_n^{\circ} [C_{e,n}(0)(C_{s,n,max} - C_{s,n}^{surf})]^{1-\alpha_n} C_{s,n}^{surf\ \alpha_n} \tag{23}$$

$$-\frac{I_L}{a_p S_p L_p n_+ F} = \{\exp[\frac{(1-\alpha_p) n_+ F \eta_p(x_p)}{RT}] - \exp[-\frac{\alpha_p n_+ F \eta_p(x_p)}{RT}]\} k_p^{\circ} [C_{e,p}(x_p) \quad (24)$$

$$(C_{s,p,max} - C_{s,p}^{surf})]^{1-\alpha_p} C_{s,p}^{surf\ \alpha_p}$$

Given a Li-ion battery load current, the lithium concentration in Li-ion battery electrode particles and the Li^+ concentration in Li-ion battery electrolytes, Eq. 23-Eq. 24 are used to compute Li-ion battery activation overpotential.

Based on Ohm's Law, Fick's First Law, Faraday's Law of Electrolysis and Nernst-Einstein Equation, the equation for computing Li-ion battery concentration overpotential is derived and written as

$$-[\zeta_p(x_p) - \zeta_n(0)] = -k_{e,d} \cdot \frac{RT[(1-t_+)/n_- + t_+/n_+]}{F} [\ln C_{e,p}(x_p) - \ln C_{e,n}(0)] \quad (25)$$

Given the Li^+ concentration in Li-ion battery electrolytes, Eq. 25 is used to compute Li-ion battery concentration overpotential. For Li-ion battery electrolytes, it is the extension of their ionic diffusion paths but not the decreases of their ionic diffusion coefficients caused by the tortuosity of their ionic conduction paths. Instead of Bruggeman coefficient, $k_{e,d}$ is introduced to modify the equation for computing Li-ion battery concentration overpotential. $k_{e,d}$ is a proportional coefficient and $k_{e,d} > 1$.

P2D model and the modified P2D model exist based on many assumptions. The differences between P2D model and the modified P2D model are reflected on Eq. 9-Eq. 11, Eq. 17-Eq. 21 and Eq. 25 [23-26]. The deriving processes of Eq. 9-Eq. 11, Eq. 21 and Eq. 25 are given in Appendix B.

3. Algorithm for computing the parameters of the modified P2D model

In this chapter, an algorithm for computing the parameters of the modified P2D model is developed. To simplify the process of computing the parameters of the modified P2D model, the parameters of the modified P2D model are merged. There are two rules for merging the parameters of the modified P2D model. First, there is one-to-one correspondence between the parameters of the modified P2D model and the modified P2D model after merging the parameters of the modified P2D model. Second, the parameters of the modified P2D model are independent after merging the parameters of the modified P2D model. Table 1 shows the parameters of the modified P2D model after merging the parameters of the modified P2D model.

Table 1

The parameters of the modified P2D model after merging the parameters of the modified P2D model.

Parameters	Expressions
e_1	$\frac{R_n^{\,2}}{D_{s,n}}$
e_2	$\frac{R_p^{\,2}}{D_{s,p}}$
e_3	$\frac{R_n}{D_{s,n}a_n S_n L_n n_+ F}$
e_4	$-\frac{R_p}{D_{s,p}a_p S_p L_p n_+ F}$
e_5	$\frac{C_{s,n,initial}}{C_{s,n,max}}$
e_6	$\frac{C_{s,p,initial}}{C_{s,p,max}}$
e_7	$\frac{(L_n + L_p + L_{sep})^2}{D_e}$
e_8	$\frac{\varepsilon_{a,n}(1-t_+)}{\varepsilon_{e,n}}$
e_9	$\frac{\varepsilon_{a,p}(1-t_+)}{\varepsilon_{e,p}}$

e_{10}	$\frac{L_n}{L_n + L_p + L_{sep}}$
e_{11}	$\frac{L_p}{L_n + L_p + L_{sep}}$
e_{12}	$\frac{\varepsilon_{e,n} S_n}{\varepsilon_{e,sep} S_{sep}}$
e_{13}	$\overline{C_e}$
e_{14}	$\frac{[(\mu^{\circ}_{\theta_{s,p}} - \mu^{\circ}_{Li\text{-}\theta_{s,p}}) - (\mu^{\circ}_{\theta_{s,n}} - \mu^{\circ}_{Li\text{-}\theta_{s,n}})] + RT \ln[(C_{s,p,max} / C_{s,p,initial} - 1) / (C_{s,n,max} / C_{s,n,initial} - 1)]}{n_+ F}$
e_{15}	$C_{s,n,max}$
e_{16}	$C_{s,p,max}$
e_{17}	$\frac{n_+ F}{RT}$
e_{18}	$R_{battery}$
e_{19}	$\frac{1}{k_n^{\circ} \overline{C_e}^{1-\alpha_n} a_n S_n L_n n_+ F}$
e_{20}	$-\frac{1}{k_p^{\circ} \overline{C_e}^{1-\alpha_p} a_p S_p L_p n_+ F}$
e_{21}	α_n
e_{22}	α_p
e_{23}	$-k_{e,d} \cdot \frac{RT[(1-t_+)/n_- + t_+/n_+]}{F} + \frac{RT}{n_+ F}$

$$\frac{[(\mu^{\circ}_{\theta_{s,p}}-\mu^{\circ}_{Li\text{-}\theta_{s,p}})-(\mu^{\circ}_{\theta_{s,n}}-\mu^{\circ}_{Li\text{-}\theta_{s,n}})]+RT\ln[(C_{s,p,max}/C_{s,p,initial}-1)/(C_{s,n,max}/C_{s,n,initial}-1)]}{n_{+}F} \tag{26}$$
$$=[ocp_p(x_p)-ocp_n(0)]_{initial}$$

$$R_{battery}=k_{s,t}\cdot(\frac{L_n}{2\sigma_n\varepsilon_{s,n}S_n}+\frac{L_p}{2\sigma_p\varepsilon_{s,p}S_p})+k_{e,t}\cdot(\frac{L_n}{2\kappa\varepsilon_{e,n}S_n}+\frac{L_p}{2\kappa\varepsilon_{e,p}S_p}+\frac{L_{sep}}{\kappa\varepsilon_{e,sep}S_{sep}})+ \tag{27}$$
$$\frac{R_nR_{SEI}}{\sigma_{SEI}a_nS_nL_n(R_n+R_{SEI})}+R_{current\ collector}$$

The parameters of the modified P2D model mentioned below refer to e_1-e_{23}. Fig. 2 shows the parameters in each mapping of the modified P2D model.

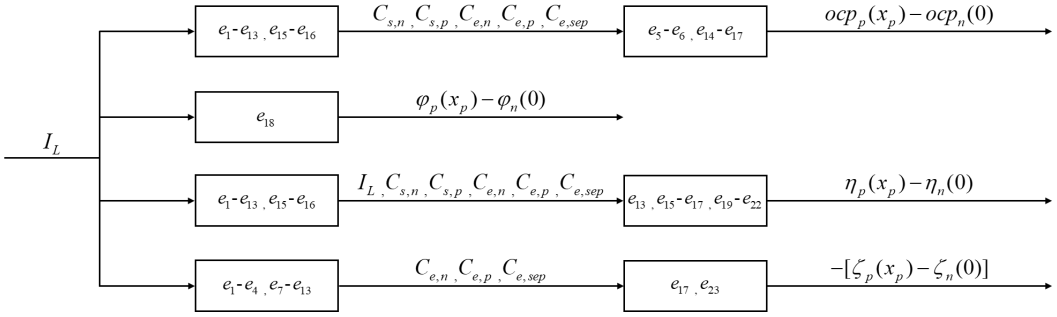

Fig. 2. The parameters in each mapping of the modified P2D model.

$$\varphi_p(x_p)-\varphi_n(0)=[\varphi_{s,p}(x_p)-\varphi_{s,n}(0)]+[\varphi_{e,p}(x_p)-\varphi_{e,n}(0)]+(-\varphi_{SEI})+ \tag{28}$$
$$(-\varphi_{current\ collector})$$

Given a set of Li-ion battery load current and Li-ion battery inter-electrode potential, the essence of computing the parameters of the modified P2D model is searching for a point at which the RMSE of the output of the modified P2D model is minimum in the 23-dimensional space. Based on the assumption that there is no local minimum in the 23-dimensional space, an algorithm for computing the parameters of the modified P2D model is developed. To describe how the algorithm for computing the parameters of the modified P2D model works clearly, an algorithm is introduced and named Example Algorithm. Example Algorithm works in the same way with the algorithm for computing the parameters of the modified P2D model but is simpler than the algorithm for computing the parameters of the modified P2D model. Therefore, how the algorithm for computing the parameters of the modified P2D model works can be reflected on how Example Algorithm works. Example Algorithm is used to solve the following problem: find a point at which x^2+y^2 is minimum in the 2-dimensional space. The problem is named Example Problem and its answer is $(0,0)$. When the answer of

Example Problem is unknown, Example Algorithm can be used to solve it. There are two modes of Example Algorithm: high-accuracy mode and high-speed mode. When Example Algorithm is in the high-accuracy mode, Example Problem can be solved with high accuracy. When Example Algorithm is in the high-speed mode, Example Problem can be solved at high speed. Fig. 3 shows the process of solving Example Problem with Example Algorithm.

(a)

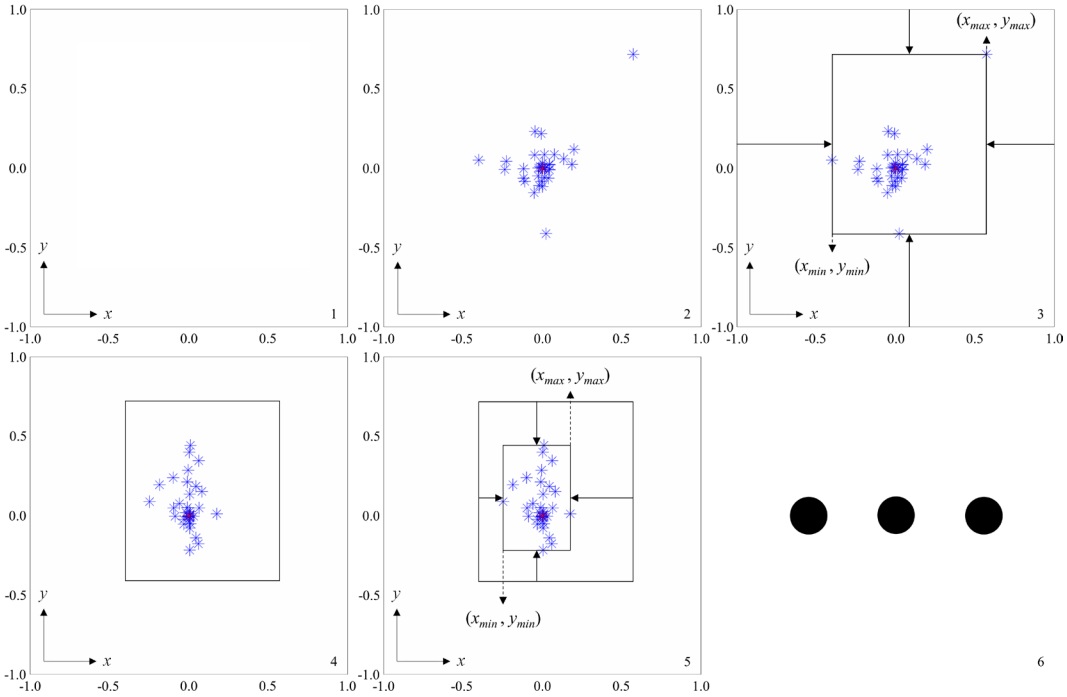

Example Algorithm is in the high-accuracy mode. 1. Set the 2-dimensional space for searching for the answer of Example Problem. 2. Generate 2-dimensional points randomly and let them move towards $(0,0)$. 3. The boundaries of the 2-dimensional space for searching for the answer of Example Problem move towards $(0,0)$. 4. Generate 2-dimensional points randomly and let them move towards $(0,0)$. 5. The boundaries of the 2-dimensional space for searching for the answer of Example Problem move towards $(0,0)$. 6. Cycle from 4.

(b)

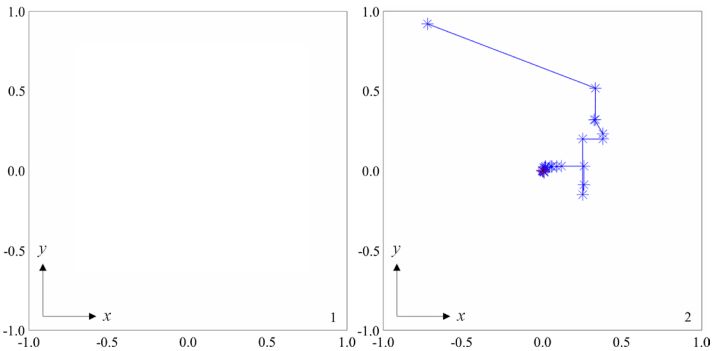

Example Algorithm is in the high-speed mode. 1. Set the 2-dimensional space for searching for the answer of Example Problem. 2. Generate a 2-dimensional point randomly and let it move towards $(0,0)$.

(c)

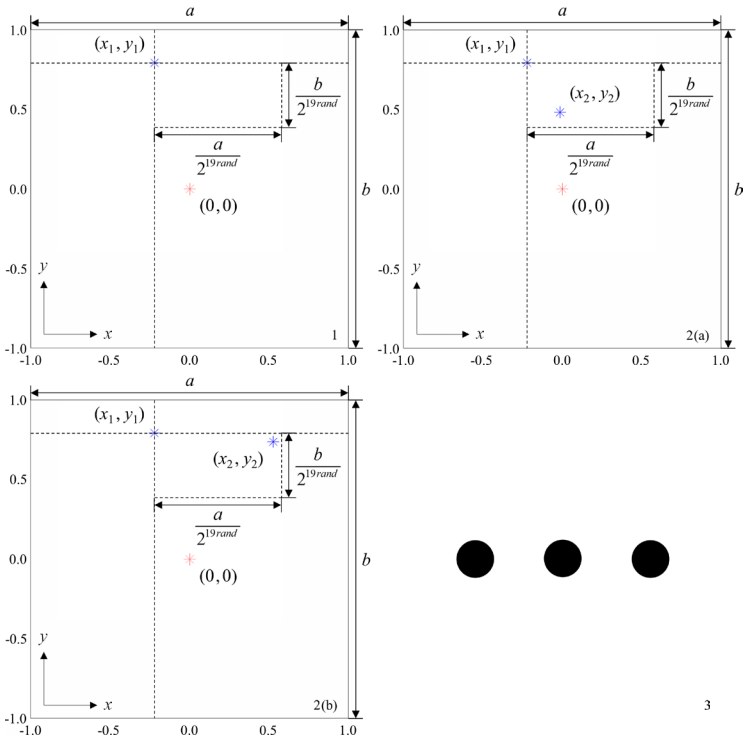

(x_1, y_1) is a 2-dimensional point generated randomly in Fig. 3a or Fig. 3b. 1. Generate 2-dimensional space randomly in the 2-dimensional space for searching for the answer of Example Problem and one of its vertexes is (x_1, y_1). 2. Generate (x_2, y_2) randomly in the 2-dimensional space generated randomly. (a)If $x_1^2 + y_1^2 > x_2^2 + y_2^2$, (x_1, y_1) moves to where (x_2, y_2) locates. (b)If $x_1^2 + y_1^2 < x_2^2 + y_2^2$, (x_1, y_1) stays put. 3. Cycle from 1.

Fig. 3. (a)The process of solving Example Problem with Example Algorithm(when Example Algorithm is in the high-accuracy mode). (b)The process of solving Example Problem with Example Algorithm(when Example Algorithm is in the high-speed mode). (c)How a 2-dimensional point moves towards $(0, 0)$ in the process of solving Example Problem.

Some points of Fig. 3 are noted as below.

1. In Fig. 3a, subscript *min* refers to minimum and subscript *max* refers to maximum. At the end of the last cycle, the 2-dimensional point which is nearest to $(0,0)$ among the 2-dimensional points is the computed answer of Example Problem when solving Example Problem with Example Algorithm and Example Algorithm is in the high-accuracy mode.

2. In Fig. 3c, *rand* refers to random. At the end of the last cycle, (x_1, y_1) is the computed answer of Example Problem when solving Example Problem with Example Algorithm and Example Algorithm is in the high-speed mode.

3. There is no difference between how a 2-dimensional point moves towards $(0, 0)$ when Example Algorithm is in the high-accuracy mode and how a 2-dimensional point moves towards $(0, 0)$ when Example Algorithm is in the high-speed mode.

The program of Example Algorithm is given in Appendix C, which is developed on

MATLAB R2020a and well-understood. Based on the program of Example Algorithm, the flow chart of Example Algorithm can be derived. Fig. 4 shows the flow chart of Example Algorithm.

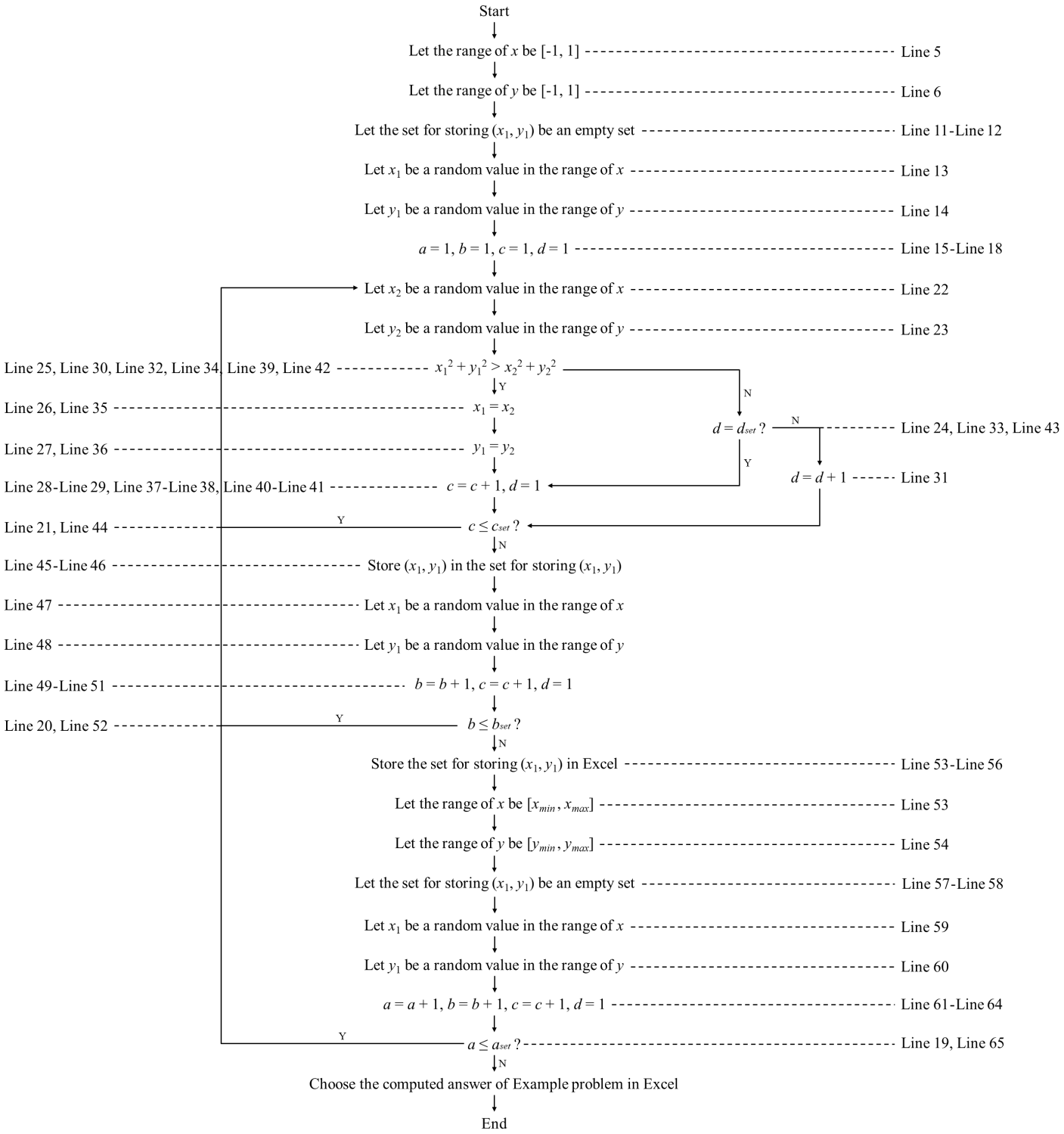

Fig. 4. The flow chart of Example Algorithm.

The parameters of Example Algorithm include a_{set}, b_{set}, c_{set} and d_{set}. a_{set} is used to

control the number of the cycles in Fig. 3a and Fig. 3b. b_{set} is used to control the number of the 2-dimensional points in Fig. 3a and Fig. 3b. When $a_{set} \neq 1$ and $b_{set} \neq 1$, Example Algorithm is in the high-accuracy mode and the process of solving Example Problem with Example Algorithm is shown in Fig. 3a. When $a_{set} = 1$ and $b_{set} = 1$, Example Algorithm is in the high-speed mode and the process of solving Example Problem with Example Algorithm is shown in Fig. 3b. c_{set} and d_{set} are used to control the number of the cycles in Fig. 3c.

The differences between Example Algorithm and the algorithm for computing the parameters of the modified P2D model are reflected on their dimensions and targets. By replacing 2-dimensional space, 2-dimensional points and $(0,0)$ with 23-dimensional space, 23-dimensional points and the values of the parameters of the modified P2D model, Example Algorithm can be converted into the algorithm for computing the parameters of the modified P2D model. The program for computing the parameters of the modified P2D model is given in Appendix C, which is developed on MATLAB R2020a.

4. Algorithm for computing the outputs of the modified P2D model

4.1 Algorithm for computing the lithium concentration in Li-ion battery electrode particles

Given a Li-ion battery load current, Eq. 1-Eq. 8 are used to compute the lithium concentration in Li-ion battery electrode particles and Eq. 1-Eq. 2 are partial differential equations. Because the analytical solutions of Eq. 1-Eq. 2 can not be computed, an algorithm for computing the lithium concentration in Li-ion battery electrode particles is developed to compute the numerical solutions of Eq. 1-Eq. 2. The algorithm for computing the lithium concentration in Li-ion battery electrode particles is derived from the finite difference method. Therefore, space and time should be discretized. Table 2 shows the parameters of the algorithm for computing the lithium concentration in Li-ion battery electrode particles.

Table 2

The parameters of the algorithm for computing the lithium concentration in Li-ion battery electrode particles.

Parameters	Definitions
$i_{s,n,max}$	The number of the space intervals along r_n axis
$i_{s,p,max}$	The number of the space intervals along r_p axis
Δt	The length of the time intervals along t axis

r_n axis and r_p axis are shown in Fig. 1a. Let i be the ordinal numbers of the space points along r_n axis or r_p axis and j be the ordinal numbers of the time points along t axis. After then, the algorithm for computing the lithium concentration in Li-ion battery electrode particles is described as below.

Eq. 1-Eq. 2 are partial differential equations. The discretization of Eq. 1-Eq. 2 yields

$$\frac{C_{s,n,i,j}-C_{s,n,i,j-1}}{\Delta t}=D_{s,n}[\frac{C_{s,n,i-1,j}-2C_{s,n,i,j}+C_{s,n,i+1,j}}{(R_n/i_{s,n,max})^2}+\frac{C_{s,n,i+1,j}-C_{s,n,i-1,j}}{i(R_n/i_{s,n,max})^2}] \quad (29)$$

$$\frac{C_{s,p,i,j}-C_{s,p,i,j-1}}{\Delta t}=D_{s,p}[\frac{C_{s,p,i-1,j}-2C_{s,p,i,j}+C_{s,p,i+1,j}}{(R_p/i_{s,p,max})^2}+\frac{C_{s,p,i+1,j}-C_{s,p,i-1,j}}{i(R_p/i_{s,p,max})^2}] \quad (30)$$

Eq. 3-Eq. 4 are initial conditions. The discretization of Eq. 3-Eq. 4 yields

$$C_{s,n,i,0} = C_{s,n,initial} \tag{31}$$

$$C_{s,p,i,0} = C_{s,p,initial} \tag{32}$$

Eq. 5-Eq. 8 are boundary conditions. The discretization of Eq. 5-Eq. 8 yields

$$-D_{s,n}\frac{C_{s,n,1,j} - C_{s,n,0,j}}{R_n / i_{s,n,max}} = 0 \tag{33}$$

$$-D_{s,p}\frac{C_{s,p,1,j} - C_{s,p,0,j}}{R_p / i_{s,p,max}} = 0 \tag{34}$$

$$-D_{s,n}\frac{C_{s,n,i_{s,n,max},j} - C_{s,n,i_{s,n,max}-1,j}}{R_n / i_{s,n,max}} = \frac{I_L}{a_n S_n L_n n_+ F} \tag{35}$$

$$-D_{s,p}\frac{C_{s,p,i_{s,p,max},j} - C_{s,p,i_{s,p,max}-1,j}}{R_p / i_{s,p,max}} = -\frac{I_L}{a_p S_p L_p n_+ F} \tag{36}$$

The transformation of Eq. 29-Eq. 30 based on Table 1 yields

$$-(1-\frac{1}{i})C_{s,n,i-1,j} + (\frac{e_1}{{i_{s,n,max}}^2\Delta t} + 2)C_{s,n,i,j} - (1+\frac{1}{i})C_{s,n,i+1,j} = \frac{e_1}{{i_{s,n,max}}^2\Delta t}C_{s,n,i,j-1} \tag{37}$$

$$-(1-\frac{1}{i})C_{s,p,i-1,j} + (\frac{e_2}{{i_{s,p,max}}^2\Delta t} + 2)C_{s,p,i,j} - (1+\frac{1}{i})C_{s,p,i+1,j} = \frac{e_2}{{i_{s,p,max}}^2\Delta t}C_{s,p,i,j-1} \tag{38}$$

The transformation of Eq. 31-Eq. 32 based on Table 1 yields

$$C_{s,n,i,0} = e_5 e_{15} \tag{39}$$

$$C_{s,p,i,0} = e_6 e_{16} \tag{40}$$

The transformation of Eq. 33-Eq. 36 based on Table 1 yields

$$-C_{s,n,0,j} + C_{s,n,1,j} = 0 \tag{41}$$

$$-C_{s,p,0,j} + C_{s,p,1,j} = 0 \tag{42}$$

$$-C_{s,n,i_{s,n,max}-1,j} + C_{s,n,i_{s,n,max},j} = -\frac{e_3}{i_{s,n,max}}I_L \tag{43}$$

$$-C_{s,p,i_{s,p,max}-1,j} + C_{s,p,i_{s,p,max},j} = -\frac{e_4}{i_{s,p,max}}I_L \tag{44}$$

Given a Li-ion battery load current, Eq. 37-Eq. 44 are used to compute the lithium concentration in Li-ion battery electrode particles. When computing the lithium concentration in Li-ion battery electrode particles at time $t+\Delta t$, I_L in Eq. 43-Eq. 44 equals to the average Li-ion battery load current between time t and time $t+\Delta t$. Eq. 37-Eq. 44 follow the law of conversation of matter, which can be proved by simulation.

4.2 Algorithm for computing the Li^+ concentration in Li-ion battery electrolytes

Given a Li-ion battery load current, Eq. 9-Eq. 16 are used to compute the Li^+ concentration in Li-ion battery electrolytes and Eq. 9-Eq. 11 are partial differential equations. Because the analytical solutions of Eq. 9-Eq. 11 can not be computed, an algorithm for computing the Li^+ concentration in Li-ion battery electrolytes is developed to compute the numerical solutions of Eq. 9-Eq. 11. The algorithm for computing the Li^+ concentration in Li-ion battery electrolytes is derived from the finite difference method. Therefore, space and time should be discretized. Table 3 shows the parameters of the algorithm for computing the Li^+ concentration in Li-ion battery electrolytes.

Table 3

The parameters of the algorithm for computing the Li^+ concentration in Li-ion battery electrolytes.

Parameters	Definitions
$i_{e,max}$	The number of the space intervals along x axis
Δt	The length of the time intervals along t axis

x axis is shown in Fig. 1a. Let i be the ordinal numbers of the space intervals along x axis and j be the ordinal numbers of the time points along t axis. After then, the algorithm for computing the Li^+ concentration in Li-ion battery electrolytes is described as below.

Eq. 9-Eq. 11 are partial differential equations. The discretization of Eq. 9-Eq. 11

yields

$$\frac{C_{e,i,j}-C_{e,i,j-1}}{\Delta t}=D_e\frac{C_{e,i-1,j}-2C_{e,i,j}+C_{e,i+1,j}}{[(L_n+L_p+L_{sep})/i_{e,max}]^2}+\frac{(1-t_+)I_L}{\varepsilon_{e,n}S_nL_nn_+F} \tag{45}$$

$$\frac{C_{e,i,j}-C_{e,i,j-1}}{\Delta t}=D_e\frac{C_{e,i-1,j}-2C_{e,i,j}+C_{e,i+1,j}}{[(L_n+L_p+L_{sep})/i_{e,max}]^2}-\frac{(1-t_+)I_L}{\varepsilon_{e,p}S_pL_pn_+F} \tag{46}$$

$$\frac{C_{e,i,j}-C_{e,i,j-1}}{\Delta t}=D_e\frac{C_{e,i-1,j}-2C_{e,i,j}+C_{e,i+1,j}}{[(L_n+L_p+L_{sep})/i_{e,max}]^2} \tag{47}$$

Based on Fick's First Law, the discretized partial differential equations for the space intervals along x axis that contain the interfaces between the electrodes and separator of a Li-ion battery are derived and written as

$$\frac{C_{e,i,j}-C_{e,i,j-1}}{\Delta t}=D_e\frac{(C_{e,i+1,j}-C_{e,i,j})\varepsilon_{e,sep}S_{sep}-(C_{e,i,j}-C_{e,i-1,j})\varepsilon_{e,n}S_n}{[(L_n+L_p+L_{sep})/i_{e,max}]^2[\varepsilon_{e,n}S_nP_n+\varepsilon_{e,sep}S_{sep}(1-P_n)]}+\frac{(1-t_+)P_nI_L}{[\varepsilon_{e,n}S_nP_n+\varepsilon_{e,sep}S_{sep}(1-P_n)]L_nn_+F} \tag{48}$$

$$\frac{C_{e,i,j}-C_{e,i,j-1}}{\Delta t}=D_e\frac{(C_{e,i+1,j}-C_{e,i,j})\varepsilon_{e,p}S_p-(C_{e,i,j}-C_{e,i-1,j})\varepsilon_{e,sep}S_{sep}}{[(L_n+L_p+L_{sep})/i_{e,max}]^2[\varepsilon_{e,p}S_pP_p+\varepsilon_{e,sep}S_{sep}(1-P_p)]}-\frac{(1-t_+)P_pI_L}{[\varepsilon_{e,p}S_pP_p+\varepsilon_{e,sep}S_{sep}(1-P_p)]L_pn_+F} \tag{49}$$

The expression of P_n in Eq. 48 is written as

$$P_n=\frac{L_n}{L_n+L_p+L_{sep}}i_{e,max}-[\frac{L_n}{L_n+L_p+L_{sep}}i_{e,max}] \tag{50}$$

The expression of P_p in Eq. 49 is written as

$$P_p=\frac{L_p}{L_n+L_p+L_{sep}}i_{e,max}-[\frac{L_p}{L_n+L_p+L_{sep}}i_{e,max}] \tag{51}$$

Eq. 12-Eq. 14 are initial conditions. The discretization of Eq. 12-Eq. 14 yields

$$C_{e,i,0}=\overline{C_e} \tag{52}$$

$$C_{e,i,0}=\overline{C_e} \tag{53}$$

$$C_{e,i,0}=\overline{C_e} \tag{54}$$

Based on Eq. 12-Eq. 14, the discretized initial conditions for the space intervals

along x axis that contain the interfaces between the electrodes and separator of a Li-ion battery are derived and written as

$$C_{e,i,0} = \overline{C_e} \tag{55}$$

$$C_{e,i,0} = \overline{C_e} \tag{56}$$

Based on Fick's First Law and Eq. 15-Eq. 16, the discretized partial differential equations for the space intervals along x axis that contain the interfaces between the electrodes and current collectors of a Li-ion battery are derived and written as

$$\frac{C_{e,1,j} - C_{e,1,j-1}}{\Delta t} = D_e \frac{-C_{e,1,j} + C_{e,2,j}}{[(L_n + L_p + L_{sep}) / i_{e,max}]^2} + \frac{(1-t_+) I_L}{\varepsilon_{e,n} S_n L_n n_+ F} \tag{57}$$

$$\frac{C_{e,i_{e,max},j} - C_{e,i_{e,max},j-1}}{\Delta t} = D_e \frac{C_{e,i_{e,max}-1,j} - C_{e,i_{e,max},j}}{[(L_n + L_p + L_{sep}) / i_{e,max}]^2} - \frac{(1-t_+) I_L}{\varepsilon_{e,p} S_p L_p n_+ F} \tag{58}$$

The transformation of Eq. 45-Eq. 47 based on Table 1 yields

$$-C_{e,i-1,j} + (\frac{e_7}{{i_{e,max}}^2 \Delta t} + 2) C_{e,i,j} - C_{e,i+1,j} = \frac{e_7}{{i_{e,max}}^2 \Delta t} C_{e,i,j-1} + \frac{e_7}{{i_{e,max}}^2} \frac{3 e_3 e_8}{e_1} I_L \tag{59}$$

$$-C_{e,i-1,j} + (\frac{e_7}{{i_{e,max}}^2 \Delta t} + 2) C_{e,i,j} - C_{e,i+1,j} = \frac{e_7}{{i_{e,max}}^2 \Delta t} C_{e,i,j-1} + \frac{e_7}{{i_{e,max}}^2} \frac{3 e_4 e_9}{e_2} I_L \tag{60}$$

$$-C_{e,i-1,j} + (\frac{e_7}{{i_{e,max}}^2 \Delta t} + 2) C_{e,i,j} - C_{e,i+1,j} = \frac{e_7}{{i_{e,max}}^2 \Delta t} C_{e,i,j-1} \tag{61}$$

The transformation of Eq. 48-Eq. 49 based on Table 1 yields

$$\begin{aligned} &-\frac{e_{12}}{e_{12} P_n + (1 - P_n)} C_{e,i-1,j} + [\frac{e_7}{{i_{e,max}}^2 \Delta t} + \frac{e_{12} + 1}{e_{12} P_n + (1 - P_n)}] C_{e,i,j} - \frac{1}{e_{12} P_n + (1 - P_n)} \\ &C_{e,i+1,j} = \frac{e_7}{{i_{e,max}}^2 \Delta t} C_{e,i,j-1} + \frac{e_7}{{i_{e,max}}^2} \frac{3 e_3 e_8}{e_1} \frac{P_n}{P_n + (1 - P_n) / e_{12}} I_L \end{aligned} \tag{62}$$

$$\begin{aligned} &-\frac{1}{e_{24} P_p + (1 - P_p)} C_{e,i-1,j} + [\frac{e_7}{{i_{e,max}}^2 \Delta t} + \frac{e_{24} + 1}{e_{24} P_p + (1 - P_p)}] C_{e,i,j} - \frac{e_{24}}{e_{24} P_p + (1 - P_p)} \\ &C_{e,i+1,j} = \frac{e_7}{{i_{e,max}}^2 \Delta t} C_{e,i,j-1} + \frac{e_7}{{i_{e,max}}^2} \frac{3 e_4 e_9}{e_2} \frac{P_p}{P_p + (1 - P_p) / e_{24}} I_L \end{aligned} \tag{63}$$

The expression of P_n in Eq. 62 is written as

$$P_n = e_{10} i_{e,max} - [e_{10} i_{e,max}] \tag{64}$$

The expression of P_p in Eq. 63 is written as

$$P_p = e_{11} i_{e,max} - [e_{11} i_{e,max}] \tag{65}$$

The expression of e_{24} in Eq. 63 is written as

$$e_{24} = -\frac{e_2 e_3 e_8 e_{10} e_{12}}{e_1 e_4 e_9 e_{11}} \tag{66}$$

The transformation of Eq. 52-Eq. 54 based on Table 1 yields

$$C_{e,i,0} = e_{13} \tag{67}$$

$$C_{e,i,0} = e_{13} \tag{68}$$

$$C_{e,i,0} = e_{13} \tag{69}$$

The transformation of Eq. 55-Eq. 56 based on Table 1 yields

$$C_{e,i,0} = e_{13} \tag{70}$$

$$C_{e,i,0} = e_{13} \tag{71}$$

The transformation of Eq. 57-Eq. 58 based on Table 1 yields

$$(\frac{e_7}{{i_{e,max}}^2 \Delta t} + 1) C_{e,1,j} - C_{e,2,j} = \frac{e_7}{{i_{e,max}}^2 \Delta t} C_{e,1,j-1} + \frac{e_7}{{i_{e,max}}^2} \frac{3 e_3 e_8}{e_1} I_L \tag{72}$$

$$-C_{e,i_{e,max}-1,j} + (\frac{e_7}{{i_{e,max}}^2 \Delta t} + 1) C_{e,i_{e,max},j} = \frac{e_7}{{i_{e,max}}^2 \Delta t} C_{e,i_{e,max},j-1} + \frac{e_7}{{i_{e,max}}^2} \frac{3 e_4 e_9}{e_2} I_L \tag{73}$$

Given a Li-ion battery load current, Eq. 59-Eq. 73 are used to compute the Li^+ concentration in Li-ion battery electrolytes. When computing the Li^+ concentration in Li-ion battery electrolytes at time $t+\Delta t$, I_L in Eq. 59-Eq. 60, Eq. 62-Eq. 63 and Eq. 72-Eq. 73 equals to the average Li-ion battery load current between time t and time $t+\Delta t$. Eq. 59 -Eq. 73 follow the law of conversation of matter, which can be proved by simulation.

4.3 Algorithm for computing Li-ion battery negative electrode activation overpotential

Given a Li-ion battery load current, the lithium concentration in Li-ion battery electrode particles and the Li^+ concentration in Li-ion battery electrolytes, Eq. 23 is

used to compute Li-ion battery negative electrode activation overpotential. Because the analytical solutions of Eq. 23 can not be computed when $\alpha_n \neq 0.5$, an algorithm for computing Li-ion battery negative electrode activation overpotential is developed to compute the numerical solutions of Eq. 23. The algorithm for computing Li-ion battery negative electrode activation overpotential is described as below.

The transformation of Eq. 23 based on Table 1 yields

$$\frac{[e_{13} / C_{e,n}(0)]^{1-e_{21}} e_{19} I_L}{(e_{15} - C_{s,n,i_{s,n,max},j})^{1-e_{21}} C_{s,n,i_{s,n,max},j}^{e_{21}}} = \exp[e_{17}(1-e_{21})\eta_n(0)] - \exp[-e_{17}e_{21}\eta_n(0)] \quad (74)$$

$e_{19} > 0$. When $I_L = 0$, the left side of Eq. 74 equals to 0. When $I_L > 0$, the left side of Eq. 74 is larger than 0. When $I_L < 0$, the left side of Eq. 74 is smaller than 0. Given a Li-ion battery load current, the lithium concentration in Li-ion battery electrode particles and the Li^+ concentration in Li-ion battery electrolytes, the essence of computing Li-ion battery negative electrode activation overpotential is searching for a point along η_n (0) axis at which the right side of Eq. 74 equals to the left side of Eq. 74. Fig. 5 shows the schematic diagram and flow chart of the algorithm for computing Li-ion battery negative electrode activation overpotential.

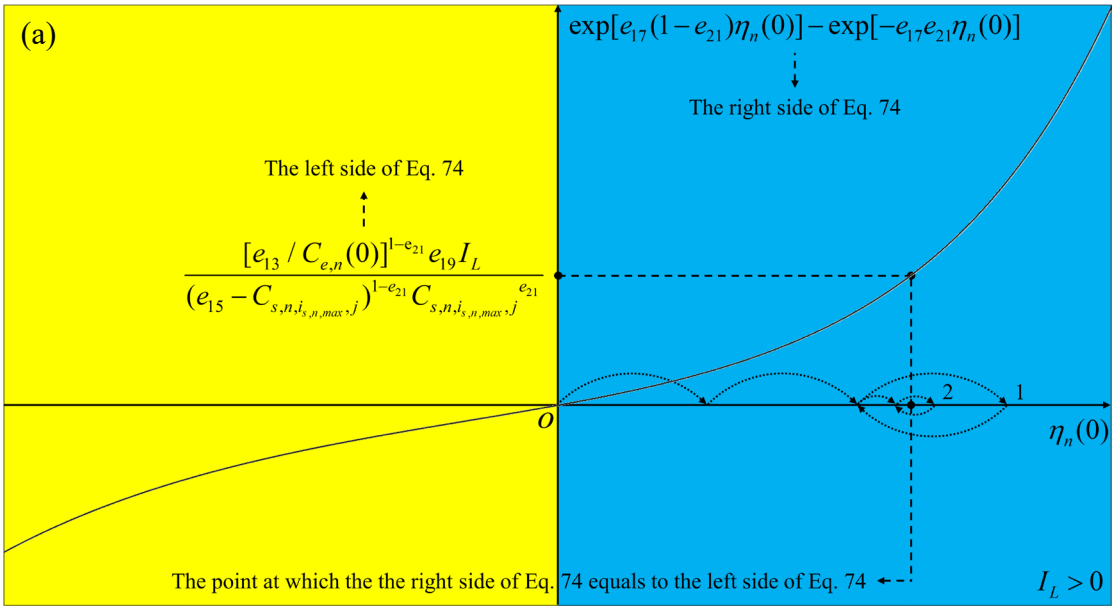

$I_L > 0$: 1. Search from $\eta_n(0) = 0$ along the positive direction of $\eta_n(0)$ axis point by point until the right side of Eq. 74 is larger than the left side of Eq. 74. The distances between each two adjacent points are equal. 2. Shorten the distances between each two adjacent points and search from the last point at which the right side of Eq. 74 is smaller than the left side of Eq. 74 along the positive direction of $\eta_n(0)$ axis point by point until the right side of Eq. 74 is larger than the left

side of Eq. 74. 3. Cycle from 2. At the end of the last cycle, return to the last point at which the right side of Eq. 74 is smaller than the left side of Eq. 74 and it is the computed Li-ion battery negative electrode activation overpotential.

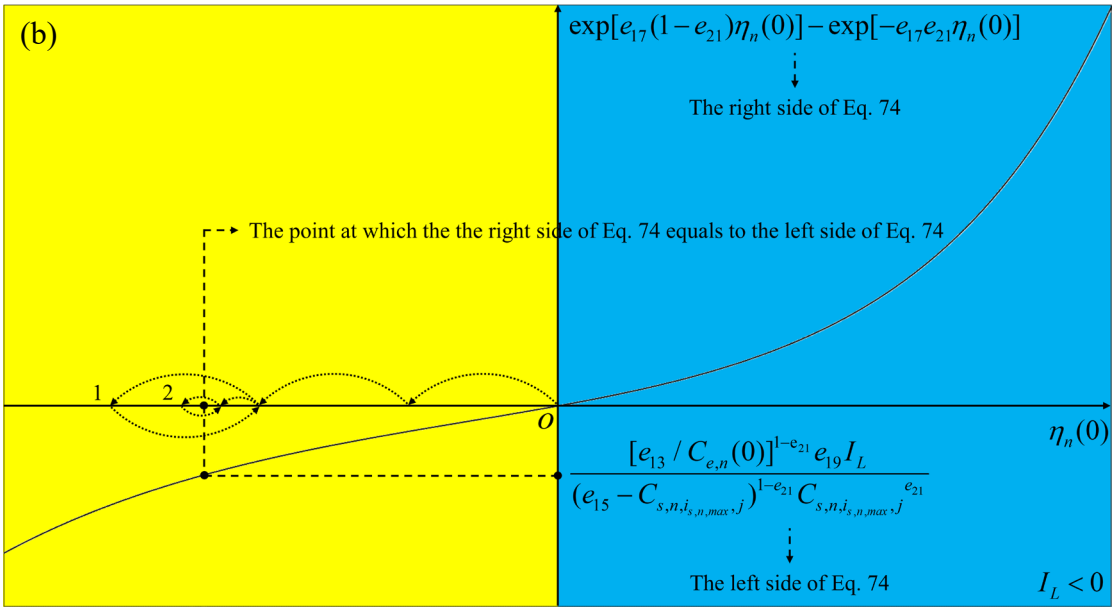

$I_L < 0$: 1. Search from $\eta_n(0) = 0$ along the negative direction of $\eta_n(0)$ axis point by point until the right side of Eq. 74 is smaller than the left side of Eq. 74. The distances between each two adjacent points are equal. 2. Shorten the distances between each two adjacent points and search from the last point at which the right side of Eq. 74 is larger than the left side of Eq. 74 along the negative direction of $\eta_n(0)$ axis point by point until the right side of Eq. 74 is smaller than the left side of Eq. 74. 3. Cycle from 2. At the end of the last cycle, return to the last point at which the right side of Eq. 74 is larger than the left side of Eq. 74 and it is the computed Li-ion battery negative electrode activation overpotential.

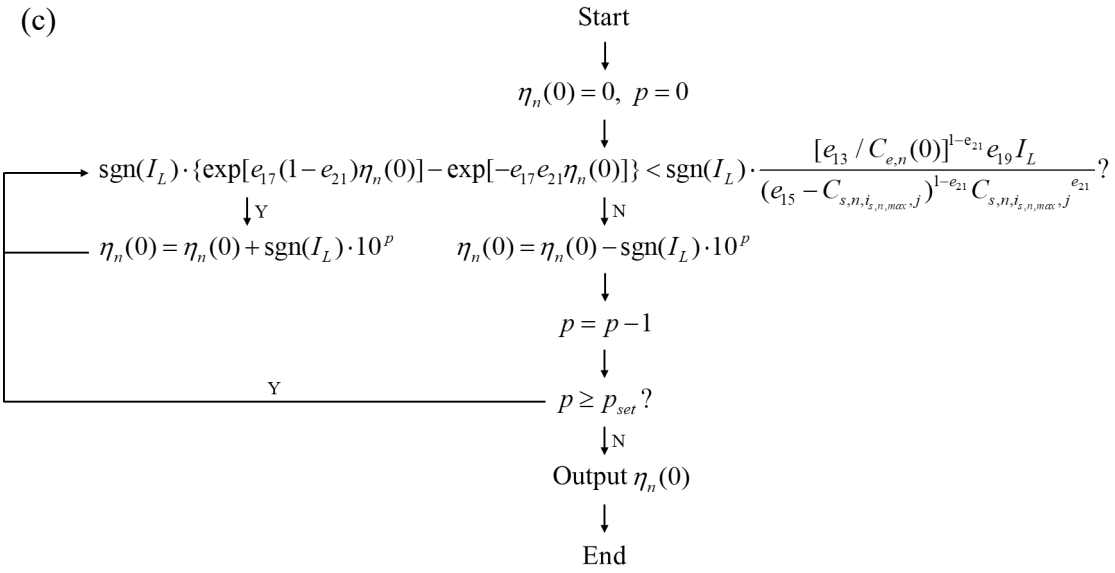

Fig. 5. (a)The schematic diagram of the algorithm for computing Li-ion battery negative electrode activation overpotential($I_L > 0$). (b)The schematic diagram of the algorithm for computing Li-ion battery negative electrode activation overpotential($I_L < 0$). (c)The flow chart of the algorithm for computing Li-ion battery negative electrode activation overpotential.

The parameter of the algorithm for computing Li-ion battery negative electrode activation overpotential is p_{set} and it is used to control the cycle number in Fig. 5a and Fig. 5b. When computing the Li-ion battery negative electrode activation overpotential at time $t+\Delta t$, I_L in Eq. 74 equals to the instantaneous Li-ion battery load current at time $t+\Delta t$.

4.4 Algorithm for computing Li-ion battery positive electrode activation overpotential

Given a Li-ion battery load current, the lithium concentration in Li-ion battery electrode particles and the Li^+ concentration in Li-ion battery electrolytes, Eq. 24 are used to compute Li-ion battery positive electrode activation overpotential. Because the analytical solution of Eq. 24 can not be computed when $\alpha_p \neq 0.5$, an algorithm for computing Li-ion battery positive electrode activation overpotential is developed to compute the numerical solution of Eq. 24. The algorithm for computing Li-ion battery positive electrode activation overpotential is described as below.

The transformation of Eq. 24 based on Table 1 yields

$$\frac{[e_{13} / C_{e,p}(x_p)]^{1-e_{22}} e_{20} I_L}{(e_{16} - C_{s,p,i_{s,p,max},j})^{1-e_{22}} C_{s,p,i_{s,p,max},j}^{e_{22}}} = \exp[e_{17}(1-e_{22})\eta_p(x_p)] - \exp[-e_{17}e_{22}\eta_p(x_p)] \quad (75)$$

$e_{20} < 0$. When $I_L = 0$, the left side of Eq. 75 equals to 0. When $I_L > 0$, the left side of Eq. 75 is smaller than 0. When $I_L < 0$, the left side of Eq. 75 is larger than 0. Given a Li-ion battery load current, the lithium concentration in Li-ion battery electrode particles and the Li^+ concentration in Li-ion battery electrolytes, the essence of computing Li-ion battery positive electrode activation overpotential is searching for a point along η_p (x_p) axis at which the right side of Eq. 75 equals to the left side of Eq. 75. Fig. 6 shows the schematic diagram and flow chart of the algorithm for computing Li-ion battery positive electrode activation overpotential.

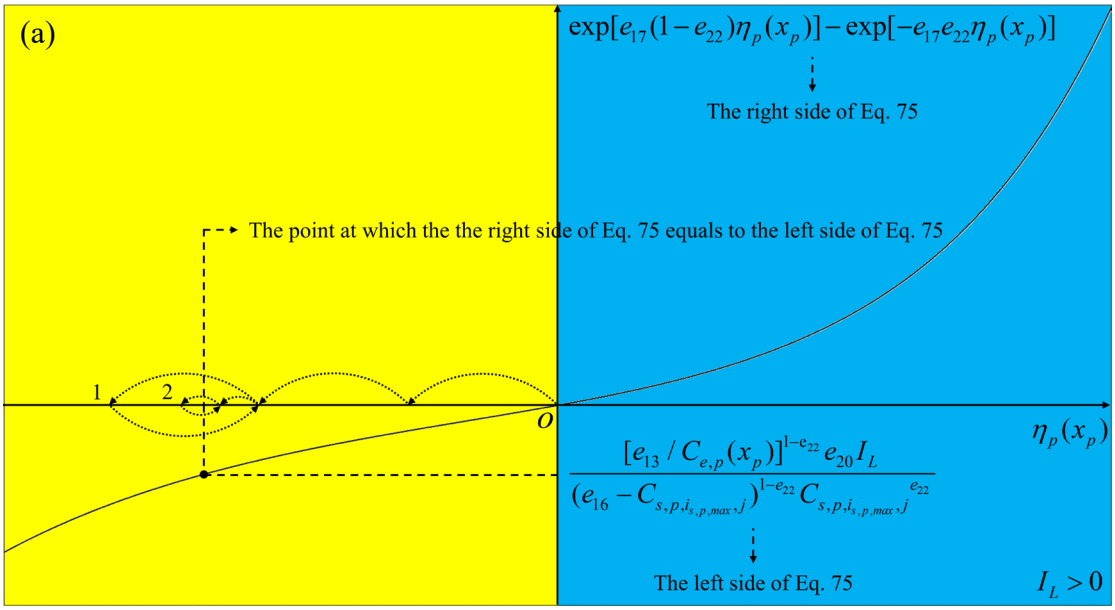

$I_L > 0$: 1. Search from $\eta_p(x_p) = 0$ along the negative direction of $\eta_p(x_p)$ axis point by point until the right side of Eq. 75 is smaller than the left side of Eq. 75. The distances between each two adjacent points are equal. 2. Shorten the distances between each two adjacent points and search from the last point at which the right side of Eq. 75 is larger than the left side of Eq. 75 along the negative direction of $\eta_p(x_p)$ axis point by point until the right side of Eq. 75 is smaller than the left side of Eq. 75. Cycle from 2. At the end of the last cycle, return to the last point at which the right side of Eq. 75 is larger than the left side of Eq. 75 and it is the computed Li-ion battery positive electrode activation overpotential.

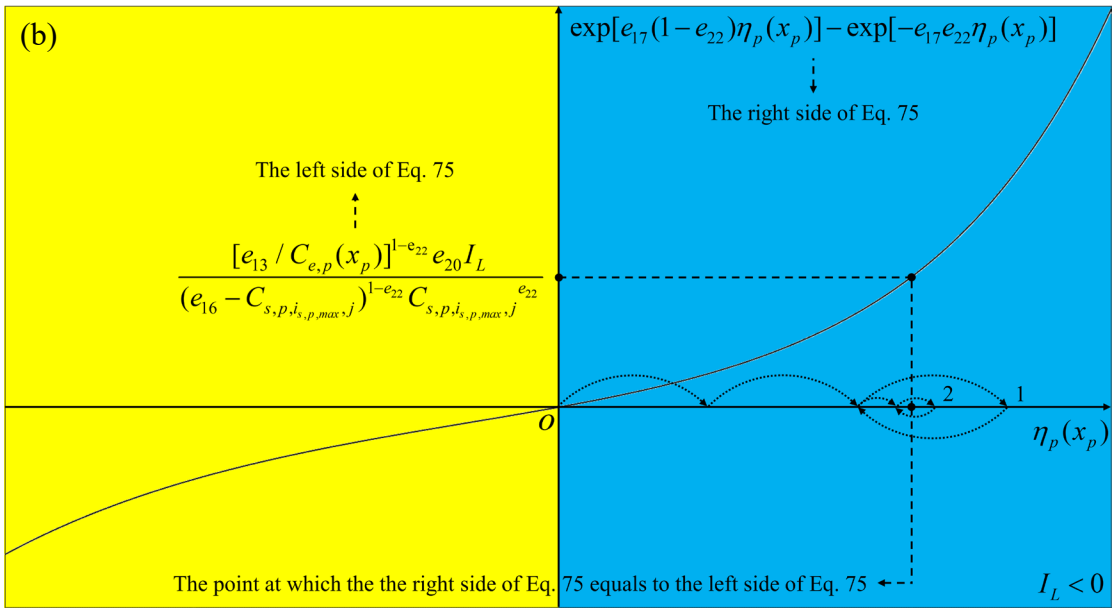

$I_L < 0$: 1. Search from $\eta_p(x_p) = 0$ along the positive direction of $\eta_p(x_p)$ axis point by point until the right side of Eq. 75 is larger than the left side of Eq. 75. The distances between each two adjacent points are equal. 2. Shorten the distances between each two adjacent points and search from the last point at which the right side of Eq. 75 is smaller than the left side of Eq. 75 along the positive direction of $\eta_p(x_p)$ axis point by point until the right side of Eq. 75 is larger than the left side of Eq. 75. 3. Cycle from 2. At the end of the last cycle, return to the last point at which the right side of Eq. 75 is smaller than the left side of Eq. 75 and it is the computed Li-ion battery positive electrode activation overpotential.

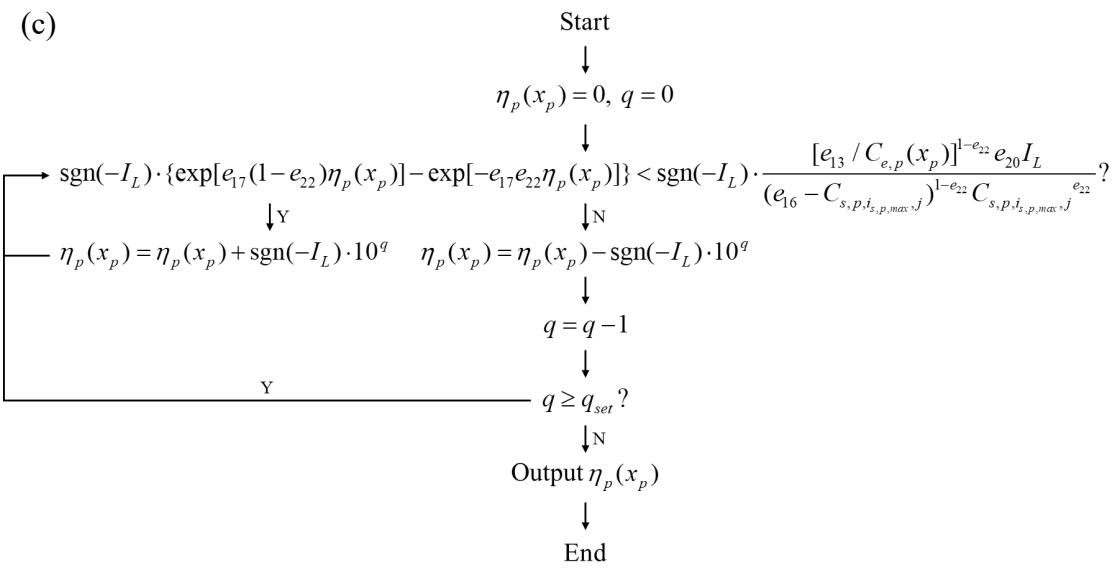

Fig. 6. (a) The schematic diagram of the algorithm for computing Li-ion battery positive electrode activation overpotential ($I_L > 0$). (b) The schematic diagram of the algorithm for computing Li-ion battery positive electrode activation overpotential ($I_L < 0$). (c) The flow chart of the algorithm for computing Li-ion battery positive electrode activation overpotential.

The parameter of the algorithm for computing Li-ion battery positive electrode activation overpotential is q_{set} and it is used to control the cycle number in Fig. 6a and Fig. 6b. When computing the Li-ion battery positive electrode activation overpotential at time $t+\Delta t$, I_L in Eq. 75 equals to the instantaneous Li-ion battery load current at time $t+\Delta t$.

The program for computing the outputs of the modified P2D model is given in Appendix C, which is developed on MATLAB R2020a.

5. Experiments and simulations

To assess the effectiveness of the modified P2D model and the algorithms for computing the parameters and outputs of the modified P2D model, experiments and simulations are conducted. Table 4 shows the experiments and simulations corresponding to different Li-ion battery types and Li-ion battery ambient temperatures.

Table 4

The experiments and simulations corresponding to different Li-ion battery types and Li-ion battery ambient temperatures.

Types	Ambient temperatures	Experiments and simulations
LG INR18650M29	283.15K	Experiment 1 1. Let the Li-ion battery stand for 1h and then measure its inter-electrode potential under Load current 1 in an incubator of 283.15K. Fig. 7a shows the graph of Load current 1. The inter-electrode potential of the Li-ion battery under Load current 1 is named Inter-electrode potential 1. Fig. 7b shows the graph of Inter-electrode potential 1. 2. Let the Li-ion battery stand for 1h and then impose Load current 1' on it in the incubator of 283.15K. The graph of Load current 1' is symmetric to the graph of Load current 1 with respect to *t* axis. 3. Let the Li-ion battery stand for 1h and then measure its inter-electrode potential under Load current 2 in the incubator of 283.15K. Fig. 7a shows the graph of Load current 2. The inter-electrode potential of the Li-ion battery under Load current 2 is named Inter-electrode potential 2. Fig. 7b shows the graph of Inter-electrode potential 2. Simulation 1 1. Given Load current 1 and Inter-electrode potential 1, compute the parameters of the modified P2D model. The computed parameters of the modified P2D model are named Parameters 1. Table 7 shows Paramters 1. Record the time for computing Parameters 1. Table 8 shows the time for computing Parameters 1. 2. Given Parameters 1 and Load current 2, compute the output of the modified P2D model. The computed output of the modified P2D model is named Output 1. Fig. 8 shows the graph of Output 1. Record the time for computing Output 1. Table 8 shows the time for computing Output 1. 3. Given Inter-electrode potential 2, compute the RMSE of Output 1. Table 8 shows the RMSE of Output 1.

LG INR18650M29	298.15K	Experiment 2 1. Let the Li-ion battery stand for 1h and then measure its inter-electrode potential under Load current 3 in an incubator of 298.15K. Fig. 7a shows the graph of Load current 3. The inter-electrode potential of the Li-ion battery under Load current 3 is named Inter-electrode potential 3. Fig. 7b shows the graph of Inter-electrode potential 3. 2. Let the Li-ion battery stand for 1h and then impose Load current 3' on it in the incubator of 298.15K. The graph of Load current 3' is symmetric to the graph of Load current 3 with respect to t axis. 3. Let the Li-ion battery stand for 1h and then measure its inter-electrode potential under Load current 4 in the incubator of 298.15K. Fig. 7a shows the graph of Load current 4. The inter-electrode potential of the Li-ion battery under Load current 4 is named Inter-electrode potential 4. Fig. 7b shows the graph of Inter-electrode potential 4.
		Simulation 2 1. Given Load current 3 and Inter-electrode potential 3, compute the parameters of the modified P2D model. The computed parameters of the modified P2D model are named Parameters 2. Table 7 shows Paramters 2. Record the time for computing Parameters 2. Table 8 shows the time for computing Parameters 2. 2. Given Parameters 2 and Load current 4, compute the output of the modified P2D model. The computed output of the modified P2D model is named Output 2. Fig. 8 shows the graph of Output 2. Record the time for computing Output 2. Table 8 shows the time for computing Output 2. 3. Given Inter-electrode potential 4, compute the RMSE of Output 2. Table 8 shows the RMSE of Output 2.

<table>
<tr><td rowspan="2">Panasonic NCR18650PF</td><td rowspan="2">318.15K</td><td>Experiment 3
1. Let the Li-ion battery stand for 1h and then measure its inter-electrode potential under Load current 5 in an incubator of 318.15K. Fig. 7a shows the graph of Load current 5. The inter-electrode potential of the Li-ion battery under Load current 5 is named Inter-electrode potential 5. Fig. 7b shows the graph of Inter-electrode potential 5.
2. Let the Li-ion battery stand for 1h and then impose Load current 5’ on it in the incubator of 318.15K. The graph of Load current 5’ is symmetric to the graph of Load current 5 with respect to t axis.
3. Let the Li-ion battery stand for 1h and then measure its inter-electrode potential under Load current 6 in the incubator of 318.15K. Fig. 7a shows the graph of Load current 6. The inter-electrode potential of the Li-ion battery under Load current 6 is named Inter-electrode potential 6. Fig. 7b shows the graph of Inter-electrode potential 6.</td></tr>
<tr><td>Simulation 3
1. Given Load current 5 and Inter-electrode potential 5, compute the parameters of the modified P2D model. The computed parameters of the modified P2D model are named Parameters 3. Table 7 shows Paramters 3. Record the time for computing Parameters 3. Table 8 shows the time for computing Parameters 3.
2. Given Parameters 3 and Load current 6, compute the output of the modified P2D model. The computed output of the modified P2D model is named Output 3. Fig. 8 shows the graph of Output 3. Record the time for computing Output 3. Table 8 shows the time for computing Output 3.
3. Given Inter-electrode potential 6, compute the RMSE of Output 3. Table 8 shows the RMSE of Output 3.</td></tr>
</table>

Panasonic NCR18650PF	333.15K	Experiment 4 1. Let the Li-ion battery stand for 1h and then measure its inter-electrode potential under Load current 7 in an incubator of 333.15K. Fig. 7a shows the graph of Load current 7. The inter-electrode potential of the Li-ion battery under Load current 7 is named Inter-electrode potential 7. Fig. 7b shows the graph of Inter-electrode potential 7. 2. Let the Li-ion battery stand for 1h and then impose Load current 7' on it in the incubator of 333.15K. The graph of Load current 7' is symmetric to the graph of Load current 7 with respect to *t* axis. 3. Let the Li-ion battery stand for 1h and then measure its inter-electrode potential under Load current 8 in the incubator of 333.15K. Fig. 7a shows the graph of Load current 8. The inter-electrode potential of the Li-ion battery under Load current 8 is named Inter-electrode potential 8. Fig. 7b shows the graph of Inter-electrode potential 8.	Simulation 4 1. Given Load current 7 and Inter-electrode potential 7, compute the parameters of the modified P2D model. The computed parameters of the modified P2D model are named Parameters 4. Table 7 shows Paramters 4. Record the time for computing Parameters 4. Table 8 shows the time for computing Parameters 4. 2. Given Parameters 4 and Load current 8, compute the output of the modified P2D model. The computed output of the modified P2D model is named Output 4. Fig. 8 shows the graph of Output 4. Record the time for computing Output 4. Table 8 shows the time for computing Output 4. 3. Given Inter-electrode potential 8, compute the RMSE of Output 4. Table 8 shows the RMSE of Output 4.

Some points of Table 4 are noted as below.

1. The experiments are conducted to obtain the data for conducting the simulations and the simulations are conducted based on the modified P2D model and the algorithms for computing the parameters and outputs of the modified P2D model. Table 5 shows the values of the parameters of the algorithm for computing the parameters of the modified

P2D model.

Table 5

The values of the parameters of the algorithm for computing the parameters of the modified P2D model.

Parameters	Values (high-accracy mode)	Values (high-speed mode)
a_{set}	5	1
b_{set}	40	1
c_{set}	400	100
d_{set}	20	20

Table 6 shows the values of the parameters of the algorithm for computing the outputs of the modified P2D model.

Table 6

The values of the parameters of the algorithm for computing the outputs of the modified P2D model.

Parameters	Values	Units
$i_{s,n,max}$	30	/
$i_{s,p,max}$	30	/
$i_{e,max}$	60	/
Δt	0.5	s
p_{set}	-15	/
q_{set}	-15	/

2. The effectiveness of the modified P2D model and the algorithms for computing the parameters and outputs of the modified P2D model are assessed based on the time for computing Parameters 1-Parameters 4, the time for computing Output 1-Output 4 and the RMSE of Output 1-Output 4.

3. The Li-ion batteries used in Experiment 1-Experiment 4 are different. In each experiment, the used Li-ion battery returns to its initial state after the second step, which is the precondition for assessing the accuracy of computing the parameters and outputs of the modified P2D model based on the RMSE of Output 1-Output 4.

Load current 1-Load current 8 are generated randomly and their complexities are different. Fig. 7 shows the graphs of Load current 1-Load current 8 and Inter-electrode potential 1-Inter-electrode potential 8.

(a)

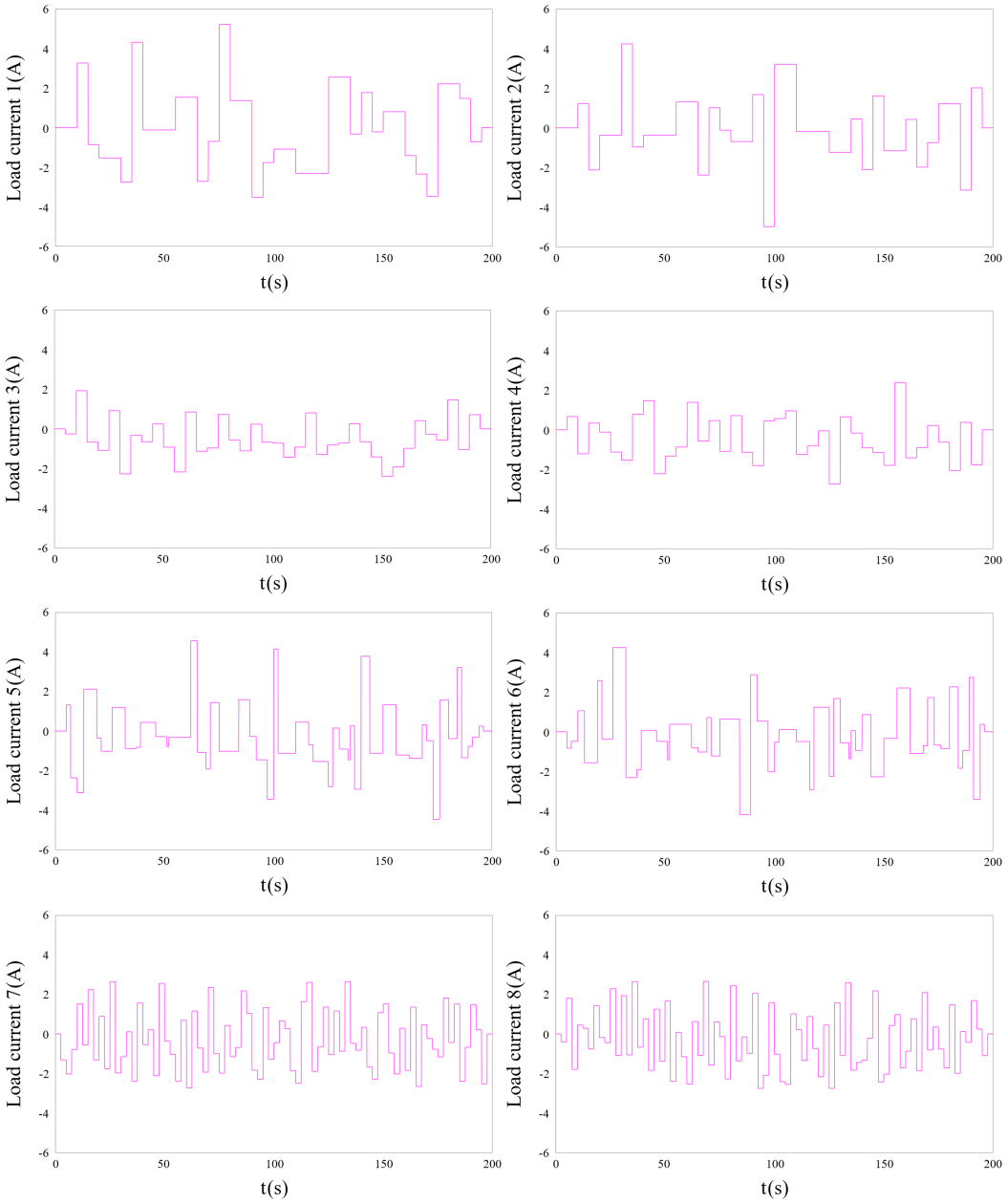

(b)

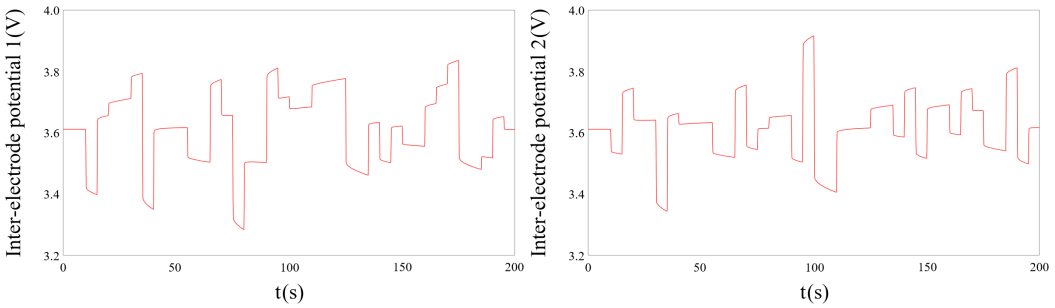

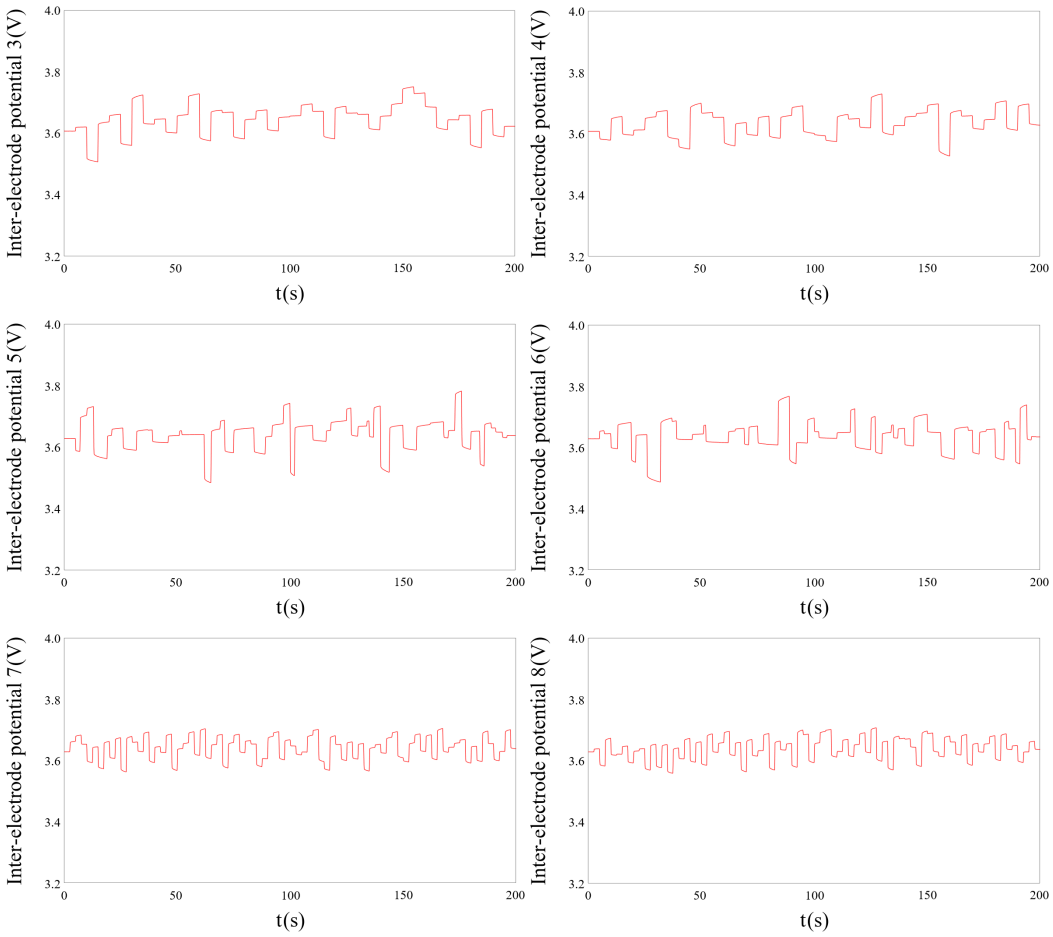

Fig. 7. (a) The graphs of Load current 1-Load current 8. (b) The graphs of Inter-electrode potential 1-Inter-electrode potential 8.

The simulations are conducted on a computer with an Intel Core i7-10750H CPU and 16 GB RAM. Table 7 shows Parameters 1-Parameters 4.

Table 7a

Parameters 1-Parameters 4 (when the algorithm for computing the parameters of the modified P2D model is in the high-accuracy mode).

Parameters	Parameters 1	Parameters 2	Parameters 3	Parameters 4
e_1	16786.5576483649	6369.52247749300	6834.82370880981	8189.91214291979
e_2	975.171928472480	412.462383423666	482.944887972188	536.231562535083
e_3	16069.2515714051	5788.53907943217	6421.05964494037	7679.59990985889
e_4	-1430.36236452818	-664.016888415346	-733.732572176168	-756.334229633261
e_5	0.310545160727765	0.326123468763074	0.385804131623773	0.307470991250392

e_6	0.645895207461160	0.617637636148637	0.578287810634101	0.641141891129840
e_7	496.829713227833	554.573677383121	644.991871898395	650.088839502127
e_8	0.482369243610940	0.524131062060952	0.411484438571639	0.409691018448880
e_9	1.65550874114124	1.77192582080428	1.70653277785168	1.54033538126800
e_{10}	0.638921006882220	0.724632440242310	0.645537063687112	0.715517147746607
e_{11}	0.116867533734035	0.125330233946968	0.110761184037795	0.150472737153683
e_{12}	0.899024181899655	0.518131553615922	0.575469319379647	0.595623550465386
e_{13}	1271.52425432868	1206.48863183176	1493.78712632566	1529.26618537301
e_{14}	3.61140000000000	3.60770000000000	3.62810000000000	3.62870000000000
e_{15}	30989.8648641201	29620.2972384230	30309.1969019125	29134.6146845317
e_{16}	45140.0504621178	48753.3935587667	48035.0727685331	44026.3412115850
e_{17}	40.5693428930227	38.6359329480396	36.0262792720764	34.2506762087030
e_{18}	0.0378281646395416	0.0167842721624810	0.0170937964642447	0.0134264902240057
e_{19}	4490.72902933724	5120.76067750397	2699.39857735979	2188.58505167351
e_{20}	-10097.4710465083	-9481.74723439062	-5893.25471683867	-3638.12252422936
e_{21}	0.555977775759452	0.549034942922364	0.615840183719546	0.381511693496819
e_{22}	0.579111206181244	0.617482681762772	0.630676230250537	0.411232925818451
e_{23}	0.171532324270083	0.134219866668602	0.146718260437841	0.113322921074871

Table 7b

Parameters 1-Parameters 4(when the algorithm for computing the parameters of the modified P2D model is in the high-speed mode).

Parameters	Parameters 1	Parameters 2	Parameters 3	Parameters 4
e_1	17288.1919971650	9503.83122041574	9283.61457225535	8625.17554789615

e_2	1113.89136151666	209.930517263752	262.134839350695	624.918718355231
e_3	16913.5786323782	8249.03869055803	8970.53607597431	7582.46068585500
e_4	-1716.21276645574	-328.602034636545	-386.457212851464	-883.488721975466
e_5	0.436407081596573	0.355072968899828	0.381334081005617	0.381960742241998
e_6	0.510482286127893	0.562454943835090	0.565347047285547	0.560202672645235
e_7	843.096071212387	480.793580582048	257.495539754953	389.483480415920
e_8	0.292763203115356	1.45989944021940	1.01358919043347	1.05994969844787
e_9	1.71502053648325	1.63248288451660	1.32883208157986	1.67503772202561
e_{10}	0.691487554512260	0.574841851339280	0.566774163234403	0.726301000943298
e_{11}	0.120929976963049	0.279098929225165	0.258044911411884	0.179176384652256
e_{12}	1.54793268396202	0.782306956084017	0.877176569443995	0.514733923040526
e_{13}	1423.12774909930	1472.36519126131	1295.55848144040	1779.95639799324
e_{14}	3.61140000000000	3.60770000000000	3.62810000000000	3.62870000000000
e_{15}	30974.5942976031	29806.2237313939	30940.9188510921	29221.7562697747
e_{16}	48464.0984775662	48340.6436677796	47111.9402788443	47048.2878763354
e_{17}	41.8976413714111	39.2087255351354	36.7088258005242	34.7416599419558
e_{18}	0.0354182840991307	0.0204608931522140	0.0124179275508791	0.00401826344653796
e_{19}	10177.8457961716	6200.06502900675	7908.41013443331	7397.13041024460
e_{20}	-7208.07716497616	-5327.01112017952	-2775.03324128100	-3871.63038367978
e_{21}	0.436986951435171	0.411108194563060	0.485198204005858	0.519254085784415
e_{22}	0.304914325394909	0.428233132613764	0.373069658118207	0.599411942776291
e_{23}	0.159630240600614	0.0747621674336658	0.0956416659362136	0.100164150657631

Fig. 8 shows the graphs of Output 1-Output 4.

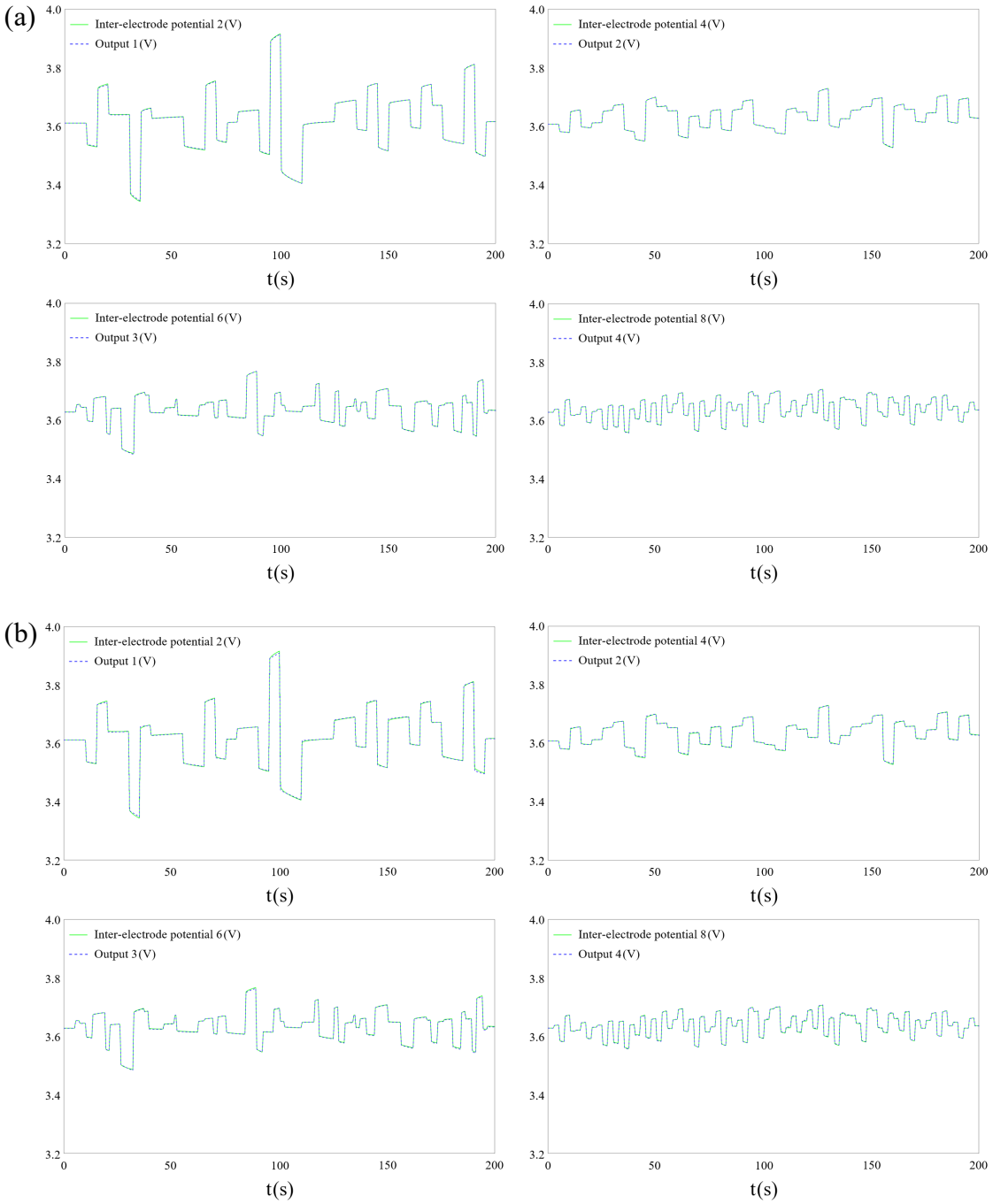

Fig. 8. (a) The graphs of Output 1-Output 4 (when the algorithm for computing the parameters of the modified P2D model is in the high-accuracy mode). (b) The graphs of Output 1- Output 4 (when the algorithm for computing the parameters of the modified P2D model is in the high-speed mode).

Table 8 shows the time for computing Parameters 1-Parameters 4, the time for computing Output 1-Output 4 and the RMSE of Output 1-Output 4.

Table 8a

The time for computing Parameters 1-Parameters 4, the time for computing Output 1-Output 4 and the RMSE of Output 1-Output 4 (when the algorithm for computing the parameters of the modified P2D model is in the high-accuracy mode).

The time for computing Parameters 1	The time for computing Output 1	The RMSE of Output 1
12h	0.079s	1.106×10^{-3} V
The time for computing Parameters 2	The time for computing Output 2	The RMSE of Output 2
12h	0.091s	4.566×10^{-4} V
The time for computing Parameters 3	The time for computing Output 3	The RMSE of Output 3
12h	0.090s	7.502×10^{-4} V
The time for computing Parameters 4	The time for computing Output 4	The RMSE of Output 4
12h	0.093s	8.546×10^{-4} V

Table 8b

The time for computing Parameters 1-Parameters 4, the time for computing Output 1-Output 4 and the RMSE of Output 1-Output 4(when the algorithm for computing the parameters of the modified P2D model is in the high-speed mode).

The time for computing Parameters 1	The time for computing Output 1	The RMSE of Output 1
33s	0.092s	1.493×10^{-3} V
The time for computing Parameters 2	The time for computing Output 2	The RMSE of Output 2
39s	0.090s	1.299×10^{-3} V
The time for computing Parameters 3	The time for computing Output 3	The RMSE of Output 3
25s	0.089s	1.566×10^{-3} V
The time for computing Parameters 4	The time for computing Output 4	The RMSE of Output 4
35s	0.086s	1.362×10^{-3} V

According to the simulation results, the modified P2D model and the algorithms for computing the parameters and outputs of the modified P2D model are effective. The time for computing Parameters 1-Parameters 4(when the algorithm for computing the parameters of the modified P2D model is in the high-accuracy mode) is longer than the time for computing Parameters 1-Parameters 4(when the algorithm for computing the parameters of the modified P2D model is in the high-speed mode) while the RMSE of Output 1-Output 4(when the algorithm for computing the parameters of the modified

P2D model is in the high-accuracy mode) is smaller than the RMSE of Output 1-Output 4(when the algorithm for computing the parameters of the modified P2D model is in the high-speed mode). If a physics-based Li-ion battery model is used to control the outputs of Li-ion batteries, its parameters should be computed in high speed. If a physics-based Li-ion battery model is used to optimize the parameters of Li-ion batteries, its parameters should be computed with high accuracy.

Some parameters of the modified P2D model do not change with Li-ion battery Li-ion battery temperature changes, SOC changes and Li-ion battery degradations, which means they do not need to be computed repeatedly. Not only Li-ion battery inter-electrode potential, but also the physical quantities in Fig. 2 can be computed based on the modified P2D model and the algorithms for computing the parameters and outputs of the modified P2D model. Given the computer for conducting simulations based on the modified P2D model and the algorithms for computing the parameters and outputs of the modified P2D model, some points of conducting simulations based on the modified P2D model and the algorithms for computing the parameters and outputs of the modified P2D model are noted as below.

1. Given the values of the parameters of the algorithms for computing the parameters and outputs of the modified P2D model, the speed of computing the parameters of the modified P2D model depends on the time length of the Li-ion battery load current for computing the parameters of the modified P2D model and the accuracy of computing the parameters of the modified P2D model depends on the complexity of the Li-ion battery load current for computing the parameters of the modified P2D model.

2. If the values of the parameters of the algorithms for computing the parameters and outputs of the modified P2D model are appropriate but the speed of computing the parameters of the modified P2D model need to be improved, decrease the time length of the Li-ion battery load current for computing the parameters of the modified P2D model to improve the speed of computing the parameters of the modified P2D model.

3. If the values of the parameters of the algorithms for computing the parameters and outputs of the modified P2D model are appropriate but the accuracy of computing the outputs of the modified P2D model is not high enough, the accuracy of computing the parameters of the modified P2D model need to be improved.

4. If the values of the parameters of the algorithms for computing the parameters and outputs of the modified P2D model are appropriate but the accuracy of computing the parameters of the modified P2D model need to be improved, increase the complexity of

the Li-ion battery load current for computing the parameters of the modified P2D model to improve the accuracy of computing the parameters of the modified P2D model.

6. Conclusions

In this paper, P2D model is modified for application. To compute the parameters and outputs of the modified P2D model fast and accurately, algorithms for computing the parameters and outputs of the modified P2D model are developed. To assess the effectiveness of the modified P2D model and the algorithms for computing the parameters and outputs of the modified P2D model, experiments and simulations are conducted. The experiments are conducted to obtain the data for conducting the simulations and the simulations are conducted based on the modified P2D model and the algorithms for computing the parameters and outputs of the modified P2D model. The simulation results are noted as below.

1. When the algorithm for computing the parameters of the modified P2D model is in the high-accuracy mode, the time for computing the parameters of the modified P2D model is 12h while the RMSE of the outputs of the modified P2D model ranges from 4.566×10^{-4}V-1.106×10^{-3}V. The time for computing the outputs of the modified P2D model ranges from 0.079s-0.093s while the time lengths of the Li-ion battery load currents for computing the outputs of the modified P2D model are 200s.

2. When the algorithm for computing the parameters of the modified P2D model is in the high-speed mode, the time for computing the parameters of the modified P2D model ranges from 25s-39s while the RMSE of the outputs of the modified P2D model ranges from 1.299×10^{-3}V-1.566×10^{-3}V. The time for computing the outputs of the modified P2D model ranges from 0.086s-0.092s while the time lengths of the Li-ion battery load currents for computing the outputs of the modified P2D model are 200s.

The simulations are conducted on a computer with an Intel Core i7-10750H CPU and 16 GB RAM. According to the simulation results, the modified P2D model and the algorithms for computing the parameters and outputs of the modified P2D model are effective. The modified P2D model are not applicable to all of Li-ion battery types, Li-ion battery states and Li-ion battery operating conditions. When the parameters of the modified P2D model change fast, the accuracy of computing the parameters of the modified P2D model will decrease. How to solve the problems is worthy of study. The modified P2D model and the algorithms for computing the parameters and outputs of

the modified P2D model can be used to develop Li-ion battery charging methods.

Acknowledgement

The work reported in the paper is financially supported by the Key-Area Research and Development Program of Guangdong Province(2023B0909030001), the National Natural Science Foundation of China(No. 52261160384, No. 52072208 and No. 223 79085), the Local Innovative and Research Teams Project of Guangdong Pearl River Talents Program(KCXST20221021111201003, JCYJ20220818101004009 and KCXF Z20211020163810015) and Shenzhen Science and Technology Program(KJZD202309 23114107014). Thank the Materials and Devices Testing Center of Tsinghua University Shenzhen International Graduate School. The technical support provided by the Materials and Devices Testing Center of Tsinghua University Shenzhen International Graduate School is professional and significant.

References

[1] A. Barré, B. Deguilhem, S. Grolleau, M. Gérard, F. Suard, D. Riu, J. Power Sources 241 (2013) 680-689.

[2] A.M. Bizeray, S. Zhao, S.R. Duncan, D.A. Howey, J. Power Sources 296 (2015) 400-412.

[3] J. Piątek, S. Afyon, T.M. Budnyak, S. Budnyk, M.H. Sipponen, A. Slabon, Adv. Energy Mater. 11 (2021) 2003456.

[4] G. Zhang, X. Wei, S. Chen, J. Zhu, G. Han, H. Dai, J. Power Sources 521 (2022) 230990.

[5] Z. Chen, D.L. Danilov, R.A. Eichel, P.H.L. Notten, Adv. Energy Mater. 12 (2022) 2201506.

[6] W. Fu, D. Kim, F. Wang, G. Yushin, J. Power Sources 561 (2023) 232738.

[7] W. Luo, C. Lyu, L. Wang, L. Zhang, J. Power Sources 241 (2013) 295-310.

[8] G. Dong, J. Wei, Electrochim. Acta 395 (2021) 139133.

[9] Y. Fan, F. Xiao, C. Li, G. Yang, X. Tang, J. Energy Storage 32 (2020) 101741.

[10] S. Siva Suriya Narayanan, S. Thangavel, J. Energy Storage 49 (2022) 104098.

[11] H. He, R. Xiong, J. Fan, Energies 4 (2011) 582-598.

[12] C. Li, N. Cui, Z. Cui, C. Wang, C. Zhang, J. Power Sources 523 (2022) 230993.

[13] M. Doyle, T.F. Fuller, J. Newman, J. Electrochem. Soc. 140 (1993) 1526-1533.

[14] A. Jokar, B. Rajabloo, M. Désilets, M. Lacroix, J. Power Sources 327 (2016) 44-55.

[15] A. Lamorgese, R. Mauri, B. Tellini, J. Energy Storage 20 (2018) 289-297.

[16] P. Nie, S. Zhang, A. Ran, C. Yang, S. Chen, Z. Li, X. Zhang, W. Deng, T. Liu, F. Kang, G. Wei, Appl. Therm. Eng. 184 (2021) 116258.

[17] S. Santhanagopalan, Q. Guo, P. Ramadass, R.E. White, J. Power Sources 156 (2006) 620-628.

[18] J. Li, N. Lotfi, R.G. Landers, J. Park, J. Electrochem. Soc. 164 (2017) A874-A883.

[19] R. Fang, H. Ge, Z. Wang, Z. Li, J. Zhang, J. Electrochem. Soc. 167 (2020) 130513.

[20] J. Li, Y. Cheng, M. Jia, Y. Tang, Y. Lin, Z. Zhang, Y. Liu, J. Power Sources 255 (2014) 130-143.

[21] J. Li, K. Adewuyi, N. Lotfi, R.G. Landers, J. Park, Appl. Energy 212 (2018) 1178-1190.

[22] S. Atalay, M. Sheikh, A. Mariani, Y. Merla, E. Bower, W. D. Widanage, J. Power Sources 478 (2020) 229026.

[23] M.D. Murbach, D.T. Schwartz, J. Electrochem. Soc. 164 (2017) E3311-E3320.

[24] Q. Zhang, D. Wang, B. Yang, X. Cui, X. Li, Electrochim. Acta 343 (2020) 136094.

[25] C. Li, N. Cui, C. Wang, C. Zhang, Energy 221 (2021) 119662.

[26] J. Kim, H. Chun, M. Kim, S. Han, J.W. Lee, T.K. Lee, J. Energy Storage 42 (2021) 103077.

Appendix A. Nomenclature

Nomenclature

a_n	Li-ion battery negative electrode specific surface area (m^{-1})
a_p	Li-ion battery positive electrode specific surface area (m^{-1})
$C_{-,n}$	Anion concentration in Li-ion battery negative electrolytes ($mol \cdot m^{-3}$)
$C_{-,p}$	Anion concentration in Li-ion battery positive electrolytes ($mol \cdot m^{-3}$)
$C_{-,sep}$	Anion concentration in Li-ion battery separator electrolytes ($mol \cdot m^{-3}$)
$C_{e,n}$	Li^+ concentration in Li-ion battery negative electrolytes ($mol \cdot m^{-3}$)
$C_{e,p}$	Li^+ concentration in Li-ion battery positive electrolytes ($mol \cdot m^{-3}$)
$C_{e,sep}$	Li^+ concentration in Li-ion battery separator electrolytes ($mol \cdot m^{-3}$)
$\overline{C_e}$	Average Li^+ concentration in Li-ion battery electrolytes ($mol \cdot m^{-3}$)
$C_{s,n}$	Li-$\theta_{s,n}$ concentration in Li-ion battery negative electrode particles ($mol \cdot m^{-3}$)
$C_{s,p}$	Li-$\theta_{s,p}$ concentration in Li-ion battery positive electrode particles ($mol \cdot m^{-3}$)
$D_{-,n}$	Anion diffusion coefficient in Li-ion battery negative electrolytes ($m^2 \cdot s^{-1}$)
$D_{-,p}$	Anion diffusion coefficient in Li-ion battery positive electrolytes ($m^2 \cdot s^{-1}$)
$D_{-,sep}$	Anion diffusion coefficient in Li-ion battery separator electrolytes ($m^2 \cdot s^{-1}$)
D_e	Li^+ diffusion coefficient in Li-ion battery electrolytes ($m^2 \cdot s^{-1}$)
$D_{e,n}$	Li^+ diffusion coefficient in Li-ion battery negative electrolytes ($m^2 \cdot s^{-1}$)
$D_{e,p}$	Li^+ diffusion coefficient in Li-ion battery positive electrolytes ($m^2 \cdot s^{-1}$)
$D_{e,sep}$	Li^+ diffusion coefficient in Li-ion battery separator electrolytes ($m^2 \cdot s^{-1}$)
$D_{s,n}$	Li-$\theta_{s,n}$ diffusion coefficient in Li-ion battery negative electrode particles ($m^2 \cdot s^{-1}$)
$D_{s,p}$	Li-$\theta_{s,p}$ diffusion coefficient in Li-ion battery positive electrode particles ($m^2 \cdot s^{-1}$)
F	Faraday's Constant ($C \cdot mol^{-1}$)
$I_{e,n}$	Li-ion battery negative electrolyte current (A)
$I_{e,p}$	Li-ion battery positive electrolyte current (A)
$I_{e,sep}$	Li-ion battery separator electrolyte current (A)
I_L	Li-ion battery load current (A)
$I_{s,n}$	Li-ion battery negative electrode current (A)
$I_{s,p}$	Li-ion battery positive electrode current (A)
$i_{s,n}$	Li-ion battery negative electrode current density ($A \cdot m^{-2}$)
$i_{s,p}$	Li-ion battery positive electrode current density ($A \cdot m^{-2}$)
j_n	Charge flux in Li-ion battery negative electrode particles ($A \cdot m^{-2}$)

j_p	Charge flux in Li-ion battery positive electrode particles ($A \cdot m^{-2}$)
$j_{Li\text{-}\theta_{s,n}}$	Li-$\theta_{s,n}$ flux in Li-ion battery negative electrode particles ($mol \cdot m^{-2} \cdot s^{-1}$)
$j_{Li\text{-}\theta_{s,p}}$	Li-$\theta_{s,p}$ flux in Li-ion battery positive electrode particles ($mol \cdot m^{-2} \cdot s^{-1}$)
k_n°	Li-ion battery negative electrode standard reaction rate constant ($m^{4-3\alpha_n} \cdot mol^{\alpha_n - 1} \cdot s^{-1}$)
k_p°	Li-ion battery positive electrode standard reaction rate constant ($m^{4-3\alpha_p} \cdot mol^{\alpha_p - 1} \cdot s^{-1}$)
L_n	Li-ion battery negative electrode thickness (m)
L_p	Li-ion battery positive electrode thickness (m)
L_{sep}	Li-ion battery separator thickness (m)
n_-	Anion charge in Li-ion battery electrolytes
n_+	Li^+ charge in Li-ion battery electrolytes
ocp_n	Li-ion battery negative electrode open circuit potential (V)
ocp_p	Li-ion battery positive electrode open circuit potential (V)
R	Universal gas constant ($J \cdot mol^{-1} \cdot K^{-1}$)
$R_{current\ collector}$	Li-ion battery current collector electronic resistance (Ω)
R_n	Li-ion battery negative electrode particle radius (m)
R_p	Li-ion battery positive electrode particle radius (m)
R_{SEI}	SEI thickness (m)
S_n	Li-ion battery negative electrode surface area (m^2)
S_p	Li-ion battery positive electrode surface area (m^2)
S_{sep}	Li-ion battery separator surface area (m^2)
$S_{eff,n}$	Li-ion battery negative electrode effective surface area (m^2)
$S_{eff,p}$	Li-ion battery positive electrode effective surface area (m^2)
T	Li-ion battery temperature (K)
t_+	Li^+ transport number in Li-ion battery electrolytes
α_n	Li-ion battery negative electrode reduction reaction transfer coefficient
α_p	Li-ion battery positive electrode reduction reaction transfer coefficient
$\varepsilon_{a,n}$	Li-ion battery negative electrode particle volume fraction
$\varepsilon_{a,p}$	Li-ion battery positive electrode particle volume fraction
$\varepsilon_{e,n}$	Li-ion battery negative electrolyte volume fraction
$\varepsilon_{e,p}$	Li-ion battery positive electrolyte volume fraction
$\varepsilon_{e,sep}$	Li-ion battery separator electrolyte volume fraction
$\varepsilon_{s,n}$	Li-ion battery negative electrode volume fraction

$\varepsilon_{s,p}$	Li-ion battery positive electrode volume fraction
$\varphi_{current\ collector}$	Li-ion battery current collector ohm overpotential (V)
$\varphi_{e,n}$	Li-ion battery negative electrolyte ohm overpotential (V)
$\varphi_{e,p}$	Li-ion battery positive electrolyte ohm overpotential (V)
$\varphi_{s,n}$	Li-ion battery negative electrode ohm overpotential (V)
$\varphi_{s,p}$	Li-ion battery positive electrode ohm overpotential (V)
φ_{SEI}	SEI ohm overpotential (V)
η_n	Li-ion battery negative electrode activation overpotential (V)
η_p	Li-ion battery positive electrode activation overpotential (V)
κ	Li-ion battery electrolyte ionic conductivity ($S \cdot m^{-1}$)
κ_n	Li-ion battery negative electrolyte ionic conductivity ($S \cdot m^{-1}$)
κ_p	Li-ion battery positive electrolyte ionic conductivity ($S \cdot m^{-1}$)
κ_{sep}	Li-ion battery separator electrolyte ionic conductivity ($S \cdot m^{-1}$)
$\mu^{\circ}_{Li^+}$	Li^+ standard chemical potential ($J \cdot mol^{-1}$)
$\mu^{\circ}_{\theta_{s,n}}$	$\theta_{s,n}$ standard chemical potential ($J \cdot mol^{-1}$)
$\mu^{\circ}_{\theta_{s,p}}$	$\theta_{s,p}$ standard chemical potential ($J \cdot mol^{-1}$)
$\mu^{\circ}_{Li\text{-}\theta_{s,n}}$	Li-$\theta_{s,n}$ standard chemical potential ($J \cdot mol^{-1}$)
$\mu^{\circ}_{Li\text{-}\theta_{s,p}}$	Li-$\theta_{s,p}$ standard chemical potential ($J \cdot mol^{-1}$)
σ_n	Li-ion battery negative electrode electronic conductivity ($S \cdot m^{-1}$)
σ_p	Li-ion battery positive electrode electronic conductivity ($S \cdot m^{-1}$)
σ_{SEI}	SEI Li^+ conductivity ($S \cdot m^{-1}$)
ζ_n	Li-ion battery negative electrolyte concentration overpotential (V)
ζ_p	Li-ion battery positive electrolyte concentration overpotential (V)
ζ_{sep}	Li-ion battery separator electrolyte concentration overpotential (V)

Superscripts

surf	Surface

Subscripts

$\theta_{s,n}$	Li-insertion site in Li-ion battery negative electrode particles
$\theta_{s,p}$	Li-insertion site in Li-ion battery positive electrode particles

Appendix B. Deriving processes of Eq. 9-Eq. 11, Eq. 21 and Eq. 25

In this chapter, Eq. 9-Eq. 11, Eq. 21 and Eq. 25 are derived. The deriving process of Eq. 9-Eq. 11 is described as below.

The reference directions of Li-ion battery load currents and Li-ion battery electrode currents are along *x* axis. Therefore, the relation between Li-ion battery load currents and Li-$\theta_{s,n}$ flux in Li-ion battery negative electrode particles is written as

$$j_{Li\text{-}\theta_{s,n}}^{surf} = \frac{I_L}{a_n S_n L_n n_+ F} \tag{76}$$

The relation between Li-ion battery load currents and Li-$\theta_{s,p}$ flux in Li-ion battery positive electrode particles is written as

$$j_{Li\text{-}\theta_{s,p}}^{surf} = -\frac{I_L}{a_p S_p L_p n_+ F} \tag{77}$$

Based on Fick's First Law, the partial differential equations for computing the Li^+ concentration in Li-ion battery electrolytes are derived and written as

$$\frac{\partial C_{e,n}}{\partial t} = \frac{[-D_e \cdot C_{e,n} / \partial x\big|_x - (-D_e \cdot C_{e,n} / \partial x\big|_{x+\partial x})] \cdot \varepsilon_{e,n} S_n + S_{eff,n}\big|_{[x,x+\partial x]} \cdot j_{Li\text{-}\theta_{s,n}}^{surf} \cdot (1-t_+)}{S_n \partial x \cdot \varepsilon_{e,n}} \tag{78}$$

$$\frac{\partial C_{e,p}}{\partial t} = \frac{[-D_e \cdot C_{e,p} / \partial x\big|_x - (-D_e \cdot C_{e,p} / \partial x\big|_{x+\partial x})] \cdot \varepsilon_{e,p} S_p + S_{eff,p}\big|_{[x,x+\partial x]} \cdot j_{Li\text{-}\theta_{s,p}}^{surf} \cdot (1-t_+)}{S_p \partial x \cdot \varepsilon_{e,p}} \tag{79}$$

$$\frac{\partial C_{e,sep}}{\partial t} = \frac{[-D_e \cdot C_{e,sep} / \partial x\big|_x - (-D_e \cdot C_{e,sep} / \partial x\big|_{x+\partial x})] \cdot \varepsilon_{e,sep} S_{sep}}{S_{sep} \partial x \cdot \varepsilon_{e,sep}} \tag{80}$$

The substitution of Eq. 76-Eq. 77 into Eq. 78-Eq. 80 yields Eq. 9-Eq. 11.

The deriving process of Eq. 21 is described as below.

The reference directions of Li-ion battery load currents and Li-ion battery electrode currents are along *x* axis. Therefore, the relation between Li-ion battery load currents and the charge flux in Li-ion battery negative electrode particles is written as

$$j_n^{surf} = \frac{I_L}{a_n S_n L_n} \tag{81}$$

Based on Ohm's Law, the equation for computing SEI ohm overpotential is derived and written as

$$-\varphi_{SEI} = -\int_{R_n}^{R_n+R_{SEI}} {R_n}^2 d\theta_n d\varphi_n j_n^{surf} \cdot \frac{dr_{SEI}}{\sigma_{SEI} {r_{SEI}}^2 d\theta_n d\varphi_n} \tag{82}$$

The substitution of Eq. 81 into Eq. 82 yields Eq. 21.

The deriving process of Eq. 25 is described as below.

Based on Ohm's Law, Fick's First Law and Faraday's Law of Electrolysis, the equation for computing Li-ion battery negative electrolyte concentration overpotential is derived and written as

$$-\frac{\partial \kappa_n \varepsilon_{e,n} S_n \zeta_n}{\partial x} = [(-D_{-,n} \frac{\partial C_{-,n}}{\partial x} \cdot n_- F) + (-D_{e,n} \frac{\partial C_{e,n}}{\partial x} \cdot n_+ F)] \cdot \varepsilon_{e,n} S_n \tag{83}$$

The equation for computing Li-ion battery positive electrolyte concentration overpotential is derived and written as

$$-\frac{\partial \kappa_p \varepsilon_{e,p} S_p \zeta_p}{\partial x} = [(-D_{-,p} \frac{\partial C_{-,p}}{\partial x} \cdot n_- F) + (-D_{e,p} \frac{\partial C_{e,p}}{\partial x} \cdot n_+ F)] \cdot \varepsilon_{e,p} S_p \tag{84}$$

The equation for computing Li-ion battery separator electrolyte concentration overpotential is derived and written as

$$-\frac{\partial \kappa_{sep} \varepsilon_{e,sep} S_{sep} \zeta_{sep}}{\partial x} = [(-D_{-,sep} \frac{\partial C_{-,sep}}{\partial x} \cdot n_- F) + (-D_{e,sep} \frac{\partial C_{e,sep}}{\partial x} \cdot n_+ F)] \cdot \varepsilon_{e,sep} S_{sep} \tag{85}$$

Based on Nernst-Einstein Equation, the relation among Li-ion battery negative electrolyte ionic conductivities and the anion diffusion coefficients in Li-ion battery negative electrolytes is derived and written as

$$D_{-,n} = \frac{RT(1-t_+)}{{n_-}^2 F^2 C_{-,n}} \kappa_n \tag{86}$$

The relation among Li-ion battery positive electrolyte ionic conductivities and the anion diffusion coefficients in Li-ion battery positive electrolytes is derived and written as

$$D_{-,p} = \frac{RT(1-t_+)}{{n_-}^2 F^2 C_{-,p}} \kappa_p \tag{87}$$

The relation among Li-ion battery separator electrolyte ionic conductivities and the anion diffusion coefficients in Li-ion battery separator electrolytes is derived and written as

$$D_{-,sep} = \frac{RT(1-t_+)}{n_-{}^2 F^2 C_{-,sep}} \kappa_{sep} \tag{88}$$

The relation among Li-ion battery negative electrolyte ionic conductivities and the Li^+ diffusion coefficients in Li-ion battery negative electrolytes is derived and written as

$$D_{e,n} = \frac{RTt_+}{n_+{}^2 F^2 C_{e,n}} \kappa_n \tag{89}$$

The relation among Li-ion battery positive electrolyte ionic conductivities and the Li^+ diffusion coefficients in Li-ion battery positive electrolytes is derived and written as

$$D_{e,p} = \frac{RTt_+}{n_+{}^2 F^2 C_{e,p}} \kappa_p \tag{90}$$

The relation among Li-ion battery separator electrolyte ionic conductivities and the Li^+ diffusion coefficients in Li-ion battery separator electrolytes is derived and written as

$$D_{e,sep} = \frac{RTt_+}{n_+{}^2 F^2 C_{e,sep}} \kappa_{sep} \tag{91}$$

Li-ion battery electrolytes are neutral. Therefore, the relation between the anion concentration in Li-ion battery negative electrolytes and the Li^+ concentration in Li-ion battery negative electrolytes is written as

$$C_{-,n} : C_{e,n} = n_+ : (-n_-) \tag{92}$$

The relation between the anion concentration in Li-ion battery positive electrolytes and the Li^+ concentration in Li-ion battery positive electrolytes is written as

$$C_{-,p} : C_{e,p} = n_+ : (-n_-) \tag{93}$$

The relation between the anion concentration in Li-ion battery separator electrolytes and the Li^+ concentration in Li-ion battery separator electrolytes is written as

$$C_{-,sep} : C_{e,sep} = n_+ : (-n_-) \tag{94}$$

The substitution of Eq. 86-Eq. 94 into Eq. 83-Eq. 85 yields

$$\frac{\partial \zeta_n}{\partial x} = \frac{RT[(1-t_+)/n_- + t_+/n_+]}{F} \frac{\partial \ln C_{e,n}}{\partial x} \tag{95}$$

$$\frac{\partial \zeta_p}{\partial x} = \frac{RT[(1-t_+)/n_- + t_+/n_+]}{F} \frac{\partial \ln C_{e,p}}{\partial x} \tag{96}$$

$$\frac{\partial \zeta_{sep}}{\partial x} = \frac{RT[(1-t_+)/n_- + t_+/n_+]}{F} \frac{\partial \ln C_{e,sep}}{\partial x} \tag{97}$$

The integration of Eq. 95 - Eq. 97 yields

$$\zeta_n(x_n) - \zeta_n(0) = \frac{RT[(1-t_+)/n_- + t_+/n_+]}{F} [\ln C_{e,n}(x_n) - \ln C_{e,n}(0)] \tag{98}$$

$$\zeta_p(x_p) - \zeta_p(x_{sep}) = \frac{RT[(1-t_+)/n_- + t_+/n_+]}{F} [\ln C_{e,p}(x_p) - \ln C_{e,p}(x_{sep})] \tag{99}$$

$$\zeta_{sep}(x_{sep}) - \zeta_{sep}(x_n) = \frac{RT[(1-t_+)/n_- + t_+/n_+]}{F} [\ln C_{e,sep}(x_{sep}) - \ln C_{e,sep}(x_n)] \tag{100}$$

At the interface between the negative electrode and separator of a Li-ion battery, the relation between the Li-ion battery negative electrolyte concentration overpotential and Li-ion battery separator electrolyte concentration overpotential is written as

$$\zeta_n(x_n) = \zeta_{sep}(x_n) \tag{101}$$

At the interface between the positive electrode and separator of a Li-ion battery, the relation between the Li-ion battery positive electrolyte concentration overpotential and Li-ion battery separator electrolyte concentration overpotential is written as

$$\zeta_p(x_{sep}) = \zeta_{sep}(x_{sep}) \tag{102}$$

Based on Eq. 101 - Eq. 102, the sum of Eq. 98 - Eq. 100 yields

$$\zeta_p(x_p) - \zeta_n(0) = \frac{RT[(1-t_+)/n_- + t_+/n_+]}{F} [\ln C_{e,p}(x_p) - \ln C_{e,n}(0)] \tag{103}$$

The transformation of Eq. 103 yields

$$-[\zeta_p(x_p) - \zeta_n(0)] = -\frac{RT[(1-t_+)/n_- + t_+/n_+]}{F} [\ln C_{e,p}(x_p) - \ln C_{e,n}(0)] \tag{104}$$

The modification of Eq. 104 with $k_{e,d}$ yields Eq. 25.

Appendix C. Program

https://data.mendeley.com/preview/j4n2gswkpk?a=a82d2c5e-1f7b-4bd5-b045-89de1e61b4a8. Include the previous works of the author and they are updated periodically. Download it after logging in to your Mendeley Data account.